

# An application of nonstandard viscosity iterative method with $s$ -convexity in the generation of fractals for rational maps

Iqbal Ahmad <sup>1,\*</sup>, Mohammed Khalid M Alnasyan <sup>2</sup>

<sup>1</sup>*Department of Mechanical Engineering, College of Engineering, Qassim University, Saudi Arabia*

<sup>2</sup>*Department of Electrical Engineering, College of Engineering, Qassim University, Saudi Arabia*

**Abstract** This paper introduces an application of novel fractal patterns, specifically Julia and Mandelbrot sets, generated by a modified class of complex rational maps in which the traditional constant term is replaced with a logarithmic component. By utilizing nonstandard viscosity iterative method with  $s$ -convexity, we derive enhanced escape criteria that refine existing computational algorithms, thereby enabling the precise visualization of intricate fractal structures as Julia and Mandelbrot sets. Our results demonstrate dynamic transformations in the shape and size of these fractals as key input parameters are adjusted. We believe that the insights garnered from this research will inspire and motivate researchers and enthusiasts deeply engaged in the field of fractal geometry.

**Keywords** Algorithms; Escape criteria; Iterative method; Julia sets; Mandelbrot sets.

**AMS 2020 subject classifications** 28A80, 37F10, 39B12, 47H10

**DOI:** 10.19139/soic-2310-5070-2871

## 1. Introduction

Fractals are infinitely complex mathematical patterns that exhibit self-similarity, meaning their intricate shapes repeat at different scales. These mesmerizing structures appear throughout nature, from the branching patterns of trees and river networks to the delicate formations of snowflakes and the spiraling arrangements of fern leaves. Mathematically, fractals are generated through iterative methods, where a simple equation or set of rules is applied repeatedly, with each iteration building upon the last to produce increasingly detailed and complex patterns. For more details, refer to [3, 12, 13, 15]. This process of repeated refinement transforms basic mathematical operations into stunningly elaborate forms that mirror the organic beauty found in the natural world. The study of fractals, particularly the visually stunning Julia and Mandelbrot sets, has captivated mathematicians for nearly a century, tracing back to the pioneering work of French mathematician Gaston Julia in the early 20th century, who first developed the fundamental concepts behind what we now call Julia sets [5]. This comprehensive approach deepens our understanding of the fundamental principles that govern natural phenomena through fractal mathematics. Through its applications, fractal geometry continues to reshape both theoretical research and creative expression, demonstrating how mathematical concepts can illuminate the beauty and structure of the universe.

The generation of fractals such as the Mandelbrot and Julia sets is fundamentally rooted in fixed-point iterative methods, with researchers utilizing diverse techniques—including Mann iteration, Picard iteration, and other advanced schemes (see [2, 10, 17, 18, 19, 16])—to explore their intricate dynamics. These iterative approaches have proven especially powerful in analyzing the behavior of polynomials, complex trigonometric functions,

---

\*Correspondence to: Iqbal Ahmad (Email: i.ahmad@qu.edu.sa). Department of Mechanical Engineering, College of Engineering, Qassim University, Saudi Arabia.

and transcendental functions, revealing how the choice of iteration method can significantly alter a fractal's visual properties—shaping its form, color patterns, and structural complexity even when applied to the same base functions (see [20, 21]). Beyond classical Julia sets, these iterative frameworks provide the mathematical foundation for generating a wide variety of other fractal types, including intricate biomorphs, iterated function system fractals, inversion fractals, and root-finding fractals (see [4, 6]), highlighting the extraordinary adaptability of iterative methods in fractal geometry. This versatility underscores how slight modifications in computational techniques can yield vastly different yet equally mesmerizing fractal structures.

The study of iterative techniques in fractal generation and analysis has undergone significant theoretical advancements, particularly through developments in viscosity approximation methods. A pivotal contribution came in 2000 with Moudafi's seminal work [11], which established crucial convergence properties of the viscosity method for semi-nonexpansive mappings, providing a rigorous mathematical framework that has profoundly shaped iterative approaches to fractal construction. This theoretical breakthrough enabled deeper analysis of fractal structures and their convergence behavior. Recent work by Nandal et al. [14] and Kumari et al. [7] has further expanded these concepts by developing generalized viscosity approximation-type iterative methods within Hilbert spaces, representing both a theoretical advancement and a practical enhancement of iterative techniques. These methodological innovations have substantially enriched fractal mathematics, yielding more sophisticated tools for investigating the complex dynamics of fractal generation while simultaneously expanding their potential applications across mathematical and computational domains.

Building on recent advancements in fractal generation, particularly the pioneering work of Tanveer et al. [20] and Iqbal et al. [1] who applied generalized viscosity approximation-type iterative methods to generate the fractals as Mandelbrot and Julia sets, this research extends their methodology to establish escape criteria for a new class of complex maps. Their innovative approach has demonstrated superior capability in capturing these fractals' intricate dynamical behavior, substantially enhancing our ability to visualize and understand their complex structural properties. Building upon these foundational developments, our current research extends this methodology by adapting viscosity approximation techniques to establish escape criteria for complex rational maps  $\mathcal{U}(z) = \Psi e^{z^p} + \frac{\Phi}{z^q} + \log \mu^\ell$  and  $\mathcal{V}(z) = \Psi \cos(z^p) + \frac{\Phi}{z^q} + \log \mu^\ell$  where  $p \geq 2, p, q \in \mathbb{N}, \Psi, \Phi \in \mathbb{C}, \mu \in \mathbb{C} \setminus \{0\}$  and  $\ell \in \mathbb{R}, \ell \geq 1$ . This extension not only broadens the theoretical framework of fractal analysis but also opens new avenues for exploring the convergence behavior and visual characteristics of fractals generated through complex logarithmic transformations.

This paper details the application of nonstandard viscosity iterative methods with  $s$ -convexity for the generation of fractals, specifically Julia and Mandelbrot sets. The study is structured into five comprehensive sections, beginning with the establishment of the necessary mathematical foundation in Section 2, which introduces the essential definitions, concepts, and preliminary results. Section 3 forms the theoretical core of our work, where we derive key theorems establishing the escape criterion as a pivotal component for constructing Julia and Mandelbrot sets via our proposed nonstandard viscosity iterative method with  $s$ -convexity for the given rational maps. Section 4 transitions to practical implementation, detailing the computational algorithms and presenting visually compelling Julia and Mandelbrot sets generated in MATLAB R2024a (version 24.1.0.2537033, 64-bit) on a standard HP laptop featuring an Intel(R) Core(TM) i7-14700HX (2.10 GHz) processor and 32 GB of RAM, with variations in parameters to demonstrate the method's versatility. Finally, Section 5 synthesizes the study's principal findings, highlighting its theoretical and computational contributions to fractal geometry.

## 2. Preliminaries

This section presents the essential definitions and preliminary results that form the basis of our work.

*Definition 2.1* (Julia set [5])

For a complex function  $\mathcal{U} : \mathbb{C} \rightarrow \mathbb{C}$  the filled Julia set  $F_{\mathcal{U}}$  is defined as:

$$F_{\mathcal{U}} = \{z \in \mathbb{C} : \{|\mathcal{U}^j(z)|\}_{p=0}^{\infty} \text{ is bounded}\}.$$

where  $\mathcal{U}^j$  denotes the  $j^{\text{th}}$  iterate of  $\mathcal{U}$ . The boundary of  $F_{\mathcal{U}}$  is called the Julia set.

*Definition 2.2* (Mandelbrot set [5])

For a complex function  $\mathcal{U} : \mathbb{C} \rightarrow \mathbb{C}$ , the Mandelbrot set  $\mathcal{M}$  is defined as:

$$\mathcal{M} = \{\mu \in \mathbb{C} : \mathcal{F}_\mu \text{ is connected}\},$$

where  $\mathcal{F}_\mu$  denotes the filled Julia set associated with Equivalently,

$$\mathcal{M} = \{\mu \in \mathbb{C} : |\mathcal{F}_\mu^j(0)| \nrightarrow \infty \text{ as } n \rightarrow \infty\}.$$

*Definition 2.3* (*s*-convex combination [16])

For complex numbers  $z_1, z_2, z_3, \dots, z_n \in \mathbb{C}$  and  $s \in (0, 1]$ , an *s*-convex combination is defined as:

$$\nu_1^s z_1 + \nu_2^s z_2 + \nu_3^s z_3 + \dots + \nu_n^s z_n.$$

where  $\nu_k \geq 0$  and  $\sum_{k=1}^n \nu_k = 1$ , for  $k \in \{1, 2, 3, \dots, n\}$ .

Let us consider the following complex mappings  $\mathcal{U}, \mathcal{V}, \mathcal{J} : \mathbb{C} \rightarrow \mathbb{C}$  as:

$$\mathcal{U}(z) = \Psi e^{z^p} + \frac{\Phi}{z^q} + \log \mu^\ell \tag{2.1}$$

$$\mathcal{V}(z) = \Psi \cos(z^p) + \frac{\Phi}{z^q} + \log \mu^\ell. \tag{2.2}$$

where  $p \geq 2, p, q \in \mathbb{N}, \Psi, \Phi \in \mathbb{C}, \mu \in \mathbb{C} \setminus \{0\}$  and  $\ell \in \mathbb{R}, \ell \geq 1$ . Moreover, let  $\mathcal{J}(z) = \wp z + \hbar$  be a complex contraction mapping with  $\wp, \hbar \in \mathbb{C}$  and  $|\wp| < 1$ .

In the article, let  $\tau = \frac{\log(\mu^\ell)}{\mu}$ . Consequently, we can express  $\log(\mu^\ell) = \tau \mu$ .

*Definition 2.4* ([13])

Let  $\{z_j\}$  be an iterative sequence with initial point  $z_0 \in \mathbb{C}$ . This sequence is called a *viscosity approximation method* if it satisfies the recurrence relation:

$$z_{j+1} = \omega_j \mathcal{J}(z_j) + (1 - \omega_j) \mathcal{U}(z_j), \quad j \geq 0,$$

where  $\mu_j \in (0, 1), \mathcal{J}, \mathcal{U} : \mathbb{C} \rightarrow \mathbb{C}$ , and moreover,  $\mathcal{J}$  is a contraction mapping.

*Definition 2.5* ([10])

Let  $\{z_j\}$  be an iterative sequence with initial point  $z_0 \in \mathbb{C}$ . This sequence is called a *viscosity approximation type iterative method* if it satisfies the coupled recurrence relations:

$$\begin{cases} z_{j+1} = \omega \mathcal{J}(z_j) + (1 - \omega) \vartheta_j, \\ \vartheta_j = \eta z_j + (1 - \eta) \mathcal{U}(z_j), \end{cases} \tag{2.3}$$

where  $\omega, \eta \in (0, 1), \mathcal{U}, \mathcal{V}, \mathcal{J} : \mathbb{C} \rightarrow \mathbb{C}$ .

The literature presents several extensions of convex combinations, including the *s*-convex combination. In this work, we integrate classical convex combinations with *s*-convex methods within the viscosity approximation orbits. Specifically, we analyze the orbit behavior of a viscosity approximation process enhanced by *s*-convexity, applied to a generalized rational complex mappings  $\mathcal{U}$  and  $\mathcal{V}$  under the contraction condition  $\mathcal{J}$  :

$$\begin{cases} z_{j+1} = \omega^s \mathcal{J}(z_j) + (1 - \omega)^s \vartheta_j, \\ \vartheta_j = \eta^s z_j + (1 - \eta)^s \mathcal{U}(z_j), \end{cases} \tag{2.4}$$

and

$$\begin{cases} z_{j+1} = \omega^s \mathcal{J}(z_j) + (1 - \omega)^s \vartheta_j, \\ \vartheta_j = \eta^s z_j + (1 - \eta)^s \mathcal{V}(z_j), \end{cases} \tag{2.5}$$

where  $z_0$  is initial point,  $\mathcal{U}$  and  $\mathcal{V}$  are complex-valued mappings,  $\mathcal{J}$  is a contraction mapping and  $\omega, \eta \in (0, 1)$  are parameters. To generate fractals and escape limitations are the basic key to run the algorithms. Since it is well known that  $|\cos(z^p)| \leq 1$  for some  $z \in \mathbb{C}$ , and the Maclaurin expansion for the cosine and exponential functions are

$$|e^{z^p}| = \left| \sum_{j=0}^{\infty} \frac{z^{jp}}{j!} \right| > \left| \sum_{j=1}^{\infty} \frac{z^{jp}}{j!} \right| = |z^p| \left| \sum_{j=1}^{\infty} \frac{z^{p(j-1)}}{j!} \right| > |\varsigma| |z^p| \tag{2.6}$$

where  $0 < |\varsigma| \leq 1$  except the values of  $z \in \mathbb{C}$  for which  $|\varsigma| = 0$ , and

$$|\cos(z^p)| = \left| \sum_{j=0}^{\infty} \frac{(-1)^j z^{2pj}}{(2j)!} \right| \geq |\xi| |z^p|, \tag{2.7}$$

where  $0 < |\xi| \leq 1$  except the values of  $z \in \mathbb{C}$  for which  $|\xi| = 0$  (see the details [?]).

### 3. Escape criteria for Mandelbrot and Julia sets

The escape criterion serves as a foundational tool in the generation and analysis of fractals, particularly for Julia sets, Mandelbrot sets, and their variants. In this work, we establish new escape criteria for a class of complex functions, enabling systematic investigation and comparison of their associated fractal sets. By employing nonstandard viscosity iterative methods with s-convexity, we explore their dynamical properties and computational behaviors.

#### 3.1. Escape criteria for $\mathcal{U}(z) = \Psi e^{z^p} + \frac{\Phi}{z^q} + \log \mu^\ell$ .

in this subsection, we derived the escape criteria for  $\mathcal{U}(z) = \Psi e^{z^p} + \frac{\Phi}{z^q} + \log \mu^\ell$  via (2.4).

##### Theorem 3.1

Assume that  $|z_0| \geq \max\{|\mu|, |\hbar|, |\Phi^{\frac{1}{p+q}}|\} > \left( \frac{(2+s\omega|\wp|+(1-s\omega)(1-s\eta)|\tau|)}{(1-s\eta)(1-s\omega)(|\Psi||\varsigma|-1)} \right)^{\frac{1}{p-1}}$ , where  $p \geq 2, p, q \in \mathbb{N}, \Psi, \Phi \in \mathbb{C}, \mu \in \mathbb{C} \setminus \{0\}$  and  $\ell \in \mathbb{R}, \ell \geq 1$ , and let  $\mathcal{J}(z) = \wp z + \hbar$  be a complex contraction mapping with  $\wp, \hbar \in \mathbb{C}$  and  $|\wp| < 1$ . If the sequence  $\{z_j\}$  is a viscosity iterative method with s-convexity defined as

$$\begin{cases} z_{j+1} = \omega^s \mathcal{J}(z_j) + (1 - \omega)^s \vartheta_j, \\ \vartheta_j = \eta^s z_j + (1 - \eta)^s \mathcal{U}(z_j). \end{cases} \tag{3.1}$$

Then, the sequence  $\{z_j\}_{j=0}^{\infty}$  diverges to infinity, i.e.,  $|z_j| \rightarrow \infty$ , as  $j \rightarrow \infty$ .

##### Proof

From (3.1), we have

$$|\vartheta_j| = |\eta^s z_j + (1 - \eta)^s \mathcal{U}(z_j)|, \quad j \geq 0.$$

For  $j = 0$ , we have

$$\begin{aligned} |\vartheta_0| &= |\eta^s z_0 + (1 - \eta)^s \mathcal{U}(z_0)| \\ &= \left| \eta^s z_0 + (1 - \eta)^s \left( \Psi e^{z_0^p} + \frac{\Phi}{z_0^q} + \log \mu^\ell \right) \right| \\ &= \left| \eta^s z_0 + (1 - \eta)^s \left( \Psi e^{z_0^p} + \frac{\Phi}{z_0^q} + \tau \mu \right) \right|. \end{aligned}$$

Since  $s, \eta \in (0, 1]$ , so  $\eta^s \geq s\eta$ , and expanding  $(1 - \eta)^s$  utilizing binomial theorem up to linear terms of  $\eta$  and using (2.6), we obtain

$$\begin{aligned} |\vartheta_0| &\geq \left| s\eta z_0 + (1 - s\eta) \left( \Psi e^{z_0^p} + \frac{\Phi}{z_0^q} + \tau\mu \right) \right| \\ &\geq (1 - s\eta) \left| \left( \Psi e^{z_0^p} + \frac{\Phi}{z_0^q} + \tau\mu \right) \right| - s\eta |z_0| \\ &\geq (1 - s\eta) |\Psi e^{z_0^p} + \tau\mu| - (1 - s\eta) \left| \frac{\Phi}{z_0^q} \right| - s\eta |z_0|, \quad s\eta < 1 \\ &\geq (1 - s\eta) |\Psi| |\varsigma| |z_0^p| - (1 - s\eta) |\tau| |\mu| - (1 - s\eta) \left| \frac{\Phi}{z_0^q} \right| - |z_0| \end{aligned}$$

Our assumption  $|z_0| \geq \max\{|\mu|, |\wp|, |\Phi|^{\frac{1}{p+q}}\}$  yields that  $-|\mu| \geq -|z_0|$  and  $|z_0| \geq |\Phi|^{\frac{1}{p+q}}$ , we obtain

$$\begin{aligned} |\vartheta_0| &\geq (1 - s\eta) |\Psi| |\varsigma| |z_0^p| - (1 - s\eta) |\tau| |z_0| - (1 - s\eta) \frac{|z_0^{p+q}|}{z_0^q} - |z_0| \\ &\geq (1 - s\eta) |\Psi| |\varsigma| |z_0^p| - (1 - s\eta) |\tau| |z_0| - (1 - s\eta) |z_0^p| - |z_0| \\ &\geq (1 - s\eta) (|\Psi| |\varsigma| - 1) |z_0^p| - (1 - s\eta) |\tau| |z_0| - s\eta |z_0| \\ &\geq |z_0| \left( (1 - s\eta) (|\Psi| |\varsigma| - 1) |z_0^{p-1}| - (1 - s\eta) |\tau| - 1 \right), \end{aligned}$$

which implies that

$$|\vartheta_0| \geq |z_0| \left( (1 - s\eta) (|\Psi| |\varsigma| - 1) |z_0^{p-1}| - (1 - s\eta) |\tau| - 1 \right). \tag{3.2}$$

Using (3.2), the binomial expansion of  $(1 - \omega)^s$  up to the first-order terms of  $\omega$ ; and the inequality  $\eta^s \geq s\eta$ , we arrive at

$$\begin{aligned} |z_1| &= |\omega^s \mathcal{J}(z_0) + (1 - \omega)^s \vartheta_0| \\ &\geq |s\omega(\wp z_0 + \hbar) + (1 - s\omega)\vartheta_0| \\ &\geq (1 - s\omega) |\vartheta_0| - s\omega |\wp z_0 + \hbar| \\ &\geq (1 - s\omega) |\vartheta_0| - s\omega |\wp| |z_0| - s\omega |\hbar| \\ &\geq (1 - s\omega) |\vartheta_0| - s\omega (1 + |\wp|) |z_0| \\ &\geq (1 - s\omega) |z_0| \left( (1 - s\eta) (|\Psi| |\varsigma| - 1) |z_0^{p-1}| - (1 - s\eta) |\tau| - 1 \right) - s\omega (1 + |\wp|) |z_0| \\ &\geq (1 - s\omega) |z_0| \left( (1 - s\eta) (|\Psi| |\varsigma| - 1) |z_0^{p-1}| - (1 - s\eta) |\tau| - 1 \right) - s\omega (1 + |\wp|) |z_0| \\ &\geq |z_0| \left( (1 - s\eta) (1 - s\omega) (|\Psi| |\varsigma| - 1) |z_0^{p-1}| - (1 - s\omega) (1 - s\eta) |\tau| - (1 - s\omega) \right. \\ &\quad \left. - s\omega (1 + |\wp|) \right) \\ &\geq |z_0| \left( (1 - s\eta) (1 - s\omega) (|\Psi| |\varsigma| - 1) |z_0^{p-1}| - (1 - s\omega) (1 - s\eta) |\tau| - (1 + s\omega |\wp|) \right). \end{aligned}$$

Our assumption  $|z_0| > \left( \frac{(2+s\omega|\wp|+(1-s\omega)(1-s\eta)|\tau|)}{(1-s\eta)(1-s\omega)(|\Psi||\varsigma|-1)} \right)^{\frac{1}{p-1}}$  gives

$$(1 - s\eta) (1 - s\omega) (|\Psi| |\varsigma| - 1) |z_0^{p-1}| - (1 - s\omega) (1 - s\eta) |\tau| - (1 + s\omega |\wp|) > 1. \tag{3.3}$$

Thus, there exists a real number  $\Gamma > 0$  such that

$$(1 - s\eta) (1 - s\omega) (|\Psi| |\varsigma| - 1) |z_0^{p-1}| - (1 - s\omega) (1 - s\eta) |\tau| - (1 + s\omega |\wp|) > 1 + \Gamma > 1.$$

From (3.3), we obtain

$$|z_1| > (1 + \Gamma)|z_0|.$$

In particular  $|z_1| > |z_0|$ . Continuing this procedure, we obtain

$$|z_j| > (1 + \Gamma)^j |z_0|.$$

Hence,  $|z_j| \rightarrow \infty$ , as  $j \rightarrow \infty$ . □

In the proof of Theorem 3.1, we have only utilized the fact that  $|z_0| \geq \max\{|\mu|, |\hbar|, |\Phi|^{\frac{1}{p+q}}\}$  and  $|z_0| \geq \left(\frac{(2+s\omega|\wp|+(1-s\omega)(1-s\eta)|\tau|)}{(1-s\eta)(1-s\omega)(|\Psi||\varsigma|-1)}\right)^{\frac{1}{p-1}}$ . So, we can refine it and obtain the following corollary.

*Corollary 3.1*

Let  $|z_0| \geq \max\left\{|\mu|, |\hbar|, |\Phi|^{\frac{1}{p+q}}, \left(\frac{(2+s\omega|\wp|+(1-s\omega)(1-s\eta)|\tau|)}{(1-s\eta)(1-s\omega)(|\Psi||\varsigma|-1)}\right)^{\frac{1}{p-1}}\right\}$ , where  $p \geq 2, p, q \in \mathbb{N}, \Psi, \Phi \in \mathbb{C}, \mu \in \mathbb{C} \setminus \{0\}$  and  $\ell \in \mathbb{R}, \ell \geq 1$ . Then  $\lim_{j \rightarrow \infty} |z_j| = \infty$ .

**3.2. Escape criteria for  $\mathcal{V}(z) = \Psi \cos(z^p) + \frac{\Phi}{z^q} + \log \mu^\ell$ .**

in this subsection, we derived the escape criteria for  $\mathcal{V}(z) = \Psi \cos(z^p) + \frac{\Phi}{z^q} + \log \mu^\ell$  via (2.5).

*Theorem 3.2*

Assume that  $|z_0| \geq \max\{|\mu|, |\hbar|, |\Phi|^{\frac{1}{p+q}}\} > \left(\frac{(2+s\omega|\wp|+(1-s\omega)(1-s\eta)|\tau|)}{(1-s\eta)(1-s\omega)(|\Psi||\varsigma|-1)}\right)^{\frac{1}{p-1}}$ , where  $p \geq 2, p, q \in \mathbb{N}, \Psi, \Phi \in \mathbb{C}, \mu \in \mathbb{C} \setminus \{0\}$  and  $\ell \in \mathbb{R}, \ell \geq 1$ , and let  $\mathcal{J}(z) = \wp z + \hbar$  be a complex contraction mapping with  $\wp, \hbar \in \mathbb{C}$  and  $|\wp| < 1$ . If the sequence  $\{z_j\}$  is a viscosity iterative method with s-convexity defined as

$$\begin{cases} z_{j+1} = \omega^s \mathcal{J}(z_j) + (1 - \omega)^s \vartheta_j, \\ \vartheta_j = \eta^s z_j + (1 - \eta)^s \mathcal{V}(z_j). \end{cases} \tag{3.4}$$

Then, the sequence  $\{z_j\}_{j=0}^\infty$  diverges to infinity, i.e.,  $|z_j| \rightarrow \infty$ , as  $j \rightarrow \infty$ .

*Proof*

From (3.4), we have

$$|\vartheta_j| = |\eta^s z_j + (1 - \eta)^s \mathcal{V}(z_j)|, \quad j \geq 0.$$

For  $j = 0$ , we have

$$\begin{aligned} |\vartheta_0| &= |\eta^s z_0 + (1 - \eta)^s \mathcal{U}(z_0)| \\ &= \left| \eta^s z_0 + (1 - \eta)^s \left( \Psi \cos(z_0^p) + \frac{\Phi}{z_0^q} + \log \mu^\ell \right) \right| \\ &= \left| \eta^s z_0 + (1 - \eta)^s \left( \Psi \cos(z_0^p) + \frac{\Phi}{z_0^q} + \tau \mu \right) \right|. \end{aligned}$$

Since  $s, \eta \in (0, 1]$ , so  $\eta^s \geq s\eta$ , and expanding  $(1 - \eta)^s$  utilizing binomial theorem up to linear terms of  $\eta$  and using (2.7), we obtain

$$\begin{aligned} |\vartheta_0| &\geq \left| s\eta z_0 + (1 - s\eta) \left( \Psi \cos(z^p_0) + \frac{\Phi}{z^q_0} + \tau\mu \right) \right| \\ &\geq (1 - s\eta) \left| \left( \Psi \cos(z^p_0) + \frac{\Phi}{z^q_0} + \tau\mu \right) \right| - s\eta|z_0| \\ &\geq (1 - s\eta) |\Psi \cos(z^p_0) + \tau\mu| - (1 - s\eta) \left| \frac{\Phi}{z^q_0} \right| - s\eta|z_0|, \quad s\eta < 1 \\ &\geq (1 - s\eta) |\Psi||\xi||z^p_0| - (1 - s\eta) |\tau||\mu| - (1 - s\eta) \frac{|\Phi|}{|z^q_0|} - |z_0| \end{aligned}$$

Our assumption  $|z_0| \geq \max\{|\mu|, |\wp|, |\Phi|^{\frac{1}{p+q}}\}$  yields that  $-|\mu| \geq -|z_0|$  and  $|z_0| \geq |\Phi|^{\frac{1}{p+q}}$ , we obtain

$$\begin{aligned} |\vartheta_0| &\geq (1 - s\eta) |\Psi||\xi||z^p| - (1 - s\eta) |\tau||z_0| - (1 - s\eta) \frac{|z^{p+q}|}{z^q_0} - |z_0| \\ &\geq (1 - s\eta) |\Psi||\xi||z^p_0| - (1 - s\eta) |\tau||z_0| - (1 - s\eta) |z^p_0| - |z_0| \\ &\geq (1 - s\eta) (|\Psi||\xi| - 1) |z^p_0| - (1 - s\eta) |\tau||z_0| - |z_0| \\ &\geq |z_0| \left( (1 - s\eta) (|\Psi||\xi| - 1) |z^{p-1}_0| - (1 - s\eta) |\tau| - 1 \right), \end{aligned}$$

which implies that

$$|\vartheta_0| \geq |z_0| \left( (1 - s\eta) (|\Psi||\xi| - 1) |z^{p-1}_0| - (1 - s\eta) |\tau| - 1 \right). \tag{3.5}$$

Using (3.5), the binomial expansion of  $(1 - \omega)^s$  up to the first-order terms of  $\omega$ ; and the inequality  $\eta^s \geq s\eta$ , we arrive at

$$\begin{aligned} |z_1| &= |\omega^s \mathcal{J}(z_0) + (1 - \omega)^s \vartheta_0| \\ &\geq |s\omega(\wp z_0 + \hbar) + (1 - s\omega)\vartheta_0| \\ &\geq (1 - s\omega) |\vartheta_0| - s\omega(1 + |\wp|) |z_0| \\ &\geq (1 - s\omega) |z_0| \left( (1 - s\eta) (|\Psi||\xi| - 1) |z^{p-1}| - (1 - s\eta) |\tau| - 1 \right) - s\omega(1 + |\wp|) |z_0| \\ &\geq |z_0| \left( (1 - s\eta)(1 - s\omega) (|\Psi||\xi| - 1) |z^{p-1}| - (1 - s\omega)(1 - s\eta) |\tau| - (1 - s\omega) \right. \\ &\quad \left. - s\omega(1 + |\wp|) \right) \\ &\geq |z_0| \left( (1 - s\eta)(1 - s\omega) (|\Psi||\xi| - 1) |z^{p-1}| - (1 - s\omega)(1 - s\eta) |\tau| - (1 + s\omega|\wp|) \right). \end{aligned}$$

Our assumption  $|z_0| > \left( \frac{(2+s\omega|\wp|+(1-s\omega)(1-s\eta)|\tau|)}{(1-s\eta)(1-s\omega)(|\Psi||\xi|-1)} \right)^{\frac{1}{p-1}}$  gives

$$(1 - s\eta)(1 - s\omega) (|\Psi||\xi| - 1) |z^{p-1}| - (1 - s\omega)(1 - s\eta) |\tau| - (1 + s\omega|\wp|) > 1. \tag{3.6}$$

Thus, there exists a real number  $\Gamma > 0$  such that

$$(1 - s\eta)(1 - s\omega) (|\Psi||\xi| - 1) |z^{p-1}| - (1 - s\omega)(1 - s\eta) |\tau| - (1 + s\omega|\wp|) > 1 + \Gamma > 1.$$

From (3.6), we obtain

$$|z_1| > (1 + \Gamma) |z_0|.$$

In particular  $|z_1| > |z_0|$ . Continuing this procedure, we obtain

$$|z_j| > (1 + \Gamma)^j |z_0|.$$

Hence,  $|z_j| \rightarrow \infty$ , as  $j \rightarrow \infty$ . □

In the proof of Theorem 3.2, we have only utilized the fact that  $|z_0| \geq \max\{|\mu|, |\hbar|, |\Phi^{\frac{1}{p+q}}|\}$  and  $|z_0| \geq \left(\frac{(2+s\omega|\varrho|+(1-s\omega)(1-s\eta)|\tau|)}{(1-s\eta)(1-s\omega)(|\Psi||\xi|-1)}\right)^{\frac{1}{p-1}}$ . So, we can refine it and obtain the following corollary.

*Corollary 3.2*

Let  $|z_0| \geq \max\left\{|\mu|, |\hbar|, |\Phi^{\frac{1}{p+q}}|, \left(\frac{(2+s\omega|\varrho|+(1-s\omega)(1-s\eta)|\tau|)}{(1-s\eta)(1-s\omega)(|\Psi||\xi|-1)}\right)^{\frac{1}{p-1}}\right\}$ , where  $p \geq 2, p, q \in \mathbb{N}, \Psi, \Phi \in \mathbb{C}, \mu \in \mathbb{C} \setminus \{0\}$  and  $\ell \in \mathbb{R}, \ell \geq 1$ . Then  $\lim_{j \rightarrow \infty} |z_j| = \infty$ .

#### 4. Application of fractals as Julia and Mandelbrot sets

By applying Corollaries 3.1 and 3.2, we construct Julia and Mandelbrot sets for the functions  $\mathcal{U}(z) = \Psi e^{z^p} + \frac{\Phi}{z^q} + \log \mu^\ell$  and  $\mathcal{V}(z) = \Psi \cos(z^p) + \frac{\Phi}{z^q} + \log \mu^\ell$ , where  $p \geq 2, p, q \in \mathbb{N}, \Psi, \Phi \in \mathbb{C}, \mu \in \mathbb{C} \setminus \{0\}$  and  $\ell \in \mathbb{R}, \ell \geq 1$ . Using a viscosity approximation method with  $s$ -convexity, we determine escape criteria: if for some if for some  $j \geq 0$ , the point  $z_j$  exceeds the radii

$$R = \max\left\{|\mu|, |\hbar|, |\Phi^{\frac{1}{p+q}}|, \left(\frac{(2 + s\omega|\varrho| + (1 - s\omega)(1 - s\eta)|\tau|)}{(1 - s\eta)(1 - s\omega)(|\Psi||\xi| - 1)}\right)^{\frac{1}{p-1}}\right\}$$

and

$$R' = \max\left\{|\mu|, |\hbar|, |\Phi^{\frac{1}{p+q}}|, \left(\frac{(2 + s\omega|\varrho| + (1 - s\omega)(1 - s\eta)|\tau|)}{(1 - s\eta)(1 - s\omega)(|\Psi||\xi| - 1)}\right)^{\frac{1}{p-1}}\right\},$$

the orbit escapes to infinity, excluding  $z_0$  from the filled Julia set. Algorithm 1 or Algorithm 3 implements an escape-time method to generate Julia sets within a region  $A \subset \mathbb{C}$  coloring points based on escape behavior, while Algorithm 2 or Algorithm 4 implements an escape-time method to generate Mandelbrot sets for  $\mathcal{U}(z)$  and  $\mathcal{V}(z)$  and checks against threshold escape radii  $R$  or  $R'$ . To avoid infinite loops, a maximum iteration limit  $K$  is imposed. Utilizing MATLAB R2024a (version 24.1.0.2537033, 64-bit) on a standard HP laptop featuring an Intel(R) Core(TM) i7-14700HX (2.10 GHz) processor and 32 GB of RAM, we visualize non-classical Julia and Mandelbrot sets, analyzing their structural variations under different parameters to efficiently capture fractal dynamics while maintaining computational feasibility. Throughout the paper, a maximum number of iterations  $K = 70$  is consistently applied.



Figure 1. A color map is used in the examples.

**4.1. Julia and Mandelbrot sets generation for  $\mathcal{U}(z) = \Psi e^{z^p} + \frac{\Phi}{z^q} + \log \mu^\ell$ .**

This subsection presents the Julia and Mandelbrot sets generated from the complex functions (2.1) under different parameter configurations via (3.1).

---

**Algorithm 1** Julia set generation for  $\mathcal{U}(z) = \Psi e^{z^p} + \frac{\Phi}{z^q} + \log \mu^\ell$

---

**Input:**  $\mathcal{U}(z) = \Psi e^{z^p} + \frac{\Phi}{z^q} + \log \mu^\ell$ , where  $p \geq 2, p, q \in \mathbb{N}, \Psi, \Phi \in \mathbb{C}, \mu \in \mathbb{C} \setminus \{0\}, \ell \geq 1$ .  
 $A \subset \mathbb{C}$ -area in which we draw the set;  $K$ -maximal number of iterations;  $\omega, \eta \in (0, 1)$ ;  
 $\mathcal{J}(z) = \wp z + \hbar$ , where  $\wp, \hbar \in \mathbb{C}$  with  $|\wp| < 1$ ; colourmap [0..C-1]-color with  $C$  colors.

**Output:** Julia set for area  $A$

**for**  $z_0 \in A$  **do**

$$\tau = \frac{\log(\mu^\ell)}{\mu}$$

$$R = \max \left\{ |\mu|, |\hbar|, \left| \Phi^{\frac{1}{p+q}} \right|, \left( \frac{(2+s\omega|\wp|+(1-s\omega)(1-s\eta)|\tau|)}{(1-s\eta)(1-s\omega)(|\Psi||\varsigma|-1)} \right)^{\frac{1}{p-1}} \right\},$$

$j = 0$

**while**  $j \leq K$  **do**

$z_{j+1} = \omega^s \mathcal{J}(z_j) + (1 - \omega)^s \vartheta_j$ ,  
 $\vartheta_j = \eta^s z_j + (1 - \eta)^s \mathcal{U}(z_j)$ , where  $0 < \omega, \eta < 1$

**if**  $|z_{j+1}| \geq R$  **then break end if**

$j = j + 1$

colour  $z_0$  with colourmap [J]

---



---

**Algorithm 2** Mandelbrot set generation for  $\mathcal{U}(z) = \Psi e^{z^p} + \frac{\Phi}{z^q} + \log \mu^\ell$

---

**Input:**  $\mathcal{U}(z) = \Psi e^{z^p} + \frac{\Phi}{z^q} + \log \mu^\ell$ , where  $p \geq 2, p, q \in \mathbb{N}, \Psi, \Phi \in \mathbb{C}, \mu \in \mathbb{C} \setminus \{0\}, \ell \geq 1$ .  
 $A \subset \mathbb{C}$ -area in which we draw the set;  $K$ -maximal number of iterations;  $\omega, \eta \in (0, 1)$ ;  
 $\mathcal{J}(z) = \wp z + \hbar$ , where  $\wp, \hbar \in \mathbb{C}$  with  $|\wp| < 1$ ; colourmap [0..C-1]-color with  $C$  colors.

**Output:** Mandelbrot set for area  $A$

**for**  $z_0 \in A$  **do**

$$\tau = \frac{\log(\mu^\ell)}{\mu}$$

$$R = \max \left\{ |\mu|, |\hbar|, \left| \Phi^{\frac{1}{p+q}} \right|, \left( \frac{(2+s\omega|\wp|+(1-s\omega)(1-s\eta)|\tau|)}{(1-s\eta)(1-s\omega)(|\Psi||\varsigma|-1)} \right)^{\frac{1}{p-1}} \right\},$$

$j = 0$

$z_0 = \mu$

**while**  $j \leq K$  **do**

$z_{j+1} = \omega^s \mathcal{J}(z_j) + (1 - \omega)^s \vartheta_j$ ,  
 $\vartheta_j = \eta^s z_j + (1 - \eta)^s \mathcal{U}(z_j)$ , where  $0 < \omega, \eta < 1$  and  $0 < s \leq 1$

**if**  $|z_{j+1}| \geq R$  **then break end if**

$j = j + 1$

colour  $z_0$  with colourmap [J]

---

In this example, we explore two scenarios: one with integer values of  $\ell$  and another with non-integer value of  $\ell$ . Using (3.1), we generate Julia sets  $\mathcal{U}(z) = \Psi e^{z^p} + \frac{\Phi}{z^q} + \log \mu^\ell$  under the following parameter choices:  $p = 2, q = 1$  and  $\varsigma = 0.5$ .

- (i) In Fig. 2: Fixed parameters  $\Psi = 0.2, \Phi = 1.1, \mu = 3i, \wp = 0.8, \hbar = 0.3, \omega = 0.1, \eta = 0.2, s = 0.7$ , and varied the value of  $\ell$  as: (a) 3, (b) 8, (c) 32, (d) 1.2, (e) 6.4, (f) 18.6.

- (iii) In Fig. 3: Fixed parameters  $\Phi = 1.1, \mu = 3i, \varphi = 0.8, \hbar = 0.3, \omega = 0.15, \eta = 0.25, s = 0.75, \ell = 4$ , and varied  $\Psi$  as: (a) 2.1, (b)  $0.21i$ , (c)  $11 + 0.21i$ .
- (iv) In Fig. 4: Fixed parameters  $\Psi = 0.11 + 0.21i, \mu = 3i, \varphi = 0.8, \hbar = 0.3, \omega = 0.15, \eta = 0.25, s = 0.75, \ell = 4$ , and varied  $\Phi$  as: (a) 6, (b)  $8.1i$ , (c)  $6 + 8.1i$ .
- (v) In Fig. 5: Fixed parameters  $\Phi = 6 + 0.21i, \Psi = 11 + .11i, \varphi = 0.1, \hbar = 0.3, \omega = 0.2, \eta = 0.3, s = 0.85, \ell = 4$ , and varied  $\mu$  as: (a) 0.7, (b)  $0.17i$ , (c)  $7 + 0.7i$ .
- (vi) In Fig. 6: Fixed parameters  $\Phi = 16 + 0.21i, \Psi = 1.1 + 11i, \mu = 0.5 + 0.7i, \hbar = 13, \omega = 0.2, \eta = 0.2, s = 0.85, \ell = 4$ , and varied  $\varphi$  as: (a) 0.6, (b)  $0.1i$ , (c)  $0.8 + 0.1i$ .
- (vii) In Fig. 7: Fixed parameters  $\Phi = 16 + 0.21i, \Psi = 1.1 + 11i, \mu = 0.5 + 0.7i, \varphi = 0.8 + 0.3i, \omega = 0.2, \eta = 0.2, s = 0.85, \ell = 4$ , and varied  $\hbar$  as: (a) 0.3, (b)  $1.3i$ , (c)  $8 + 3i$ .

The Julia sets illustrated in Figures 2-7 (a, b, c), generated for a spectrum of values assigned to the parameters  $\ell, \Psi, \Phi, \mu, \varphi, \hbar$ , reveal the profound and nuanced influence these factors exert on the resulting fractal structures. In Figure 2 (a-f), specifically, sub-figures (a-c) depict the sets when  $\ell$  is fixed as an integer, while sub-figures (d-f) show the sets for non-integer values of  $\ell$ . It is evident that the parameter  $\ell$  significantly influences the shape of the Julia sets, even slight variations in  $\ell$  can lead to substantial changes in their structure. Clearly demonstrating that this parameter is a primary determinant of morphological identity, as even minimal alterations in its value precipitate significant topological transformations. A consistent axial symmetry along the real axis is observed across all variations. Furthermore, a secondary trend emerges wherein a gradual increase in  $\ell$  corresponds to a systematic reduction in the dimensions of the prominent bulb-like formations, underscoring the parameter's nuanced role in shaping the fractal geometry. In contrast, Figures 2 (a-f) display axial symmetry along the real axis. Upon closer inspection, we observe that the size of the bulb-like structures in the sets gradually decreases as the value of  $\ell$  increases. Additionally, Figures 3-7 (a, b, c) in subfigures (a), the parameters are set as purely real, in (b) as purely imaginary, and in (c) as complex values. These variations highlight the significant influence of  $\Psi, \Phi, \mu, \varphi, \hbar$  on the geometry, scale, and coloration of the Julia sets particularly around the edges of the characteristic leaf-like structures. The image generation time for each iteration is also recorded.

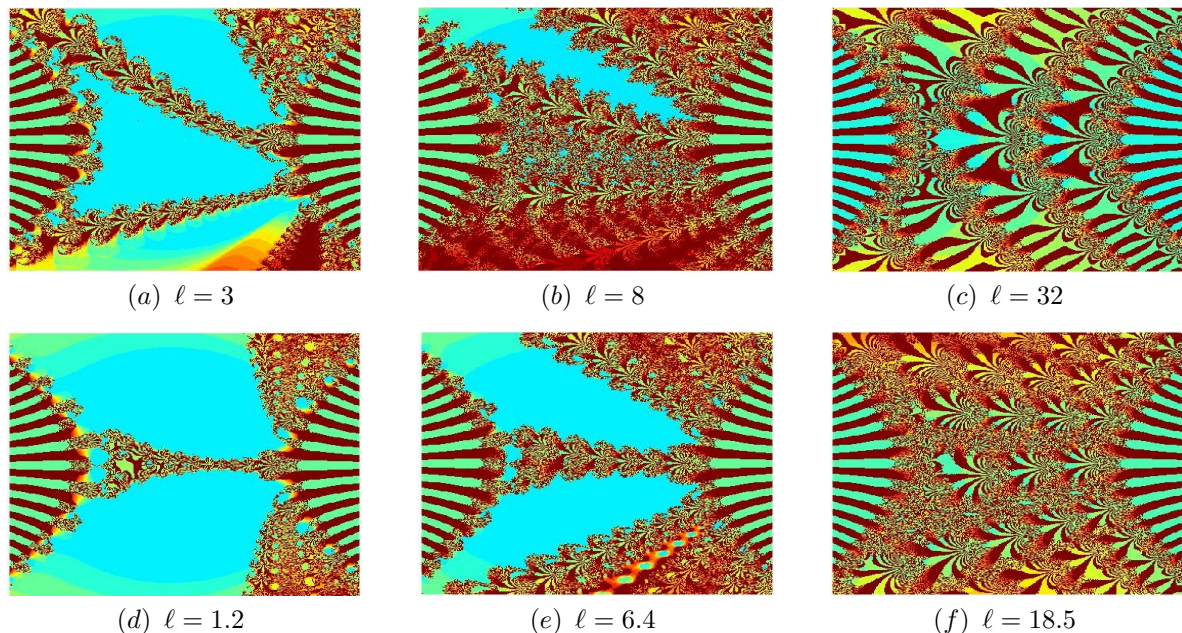


Figure 2. Julia sets generated via Algorithm 1 for varying values of  $\ell$ , with execution times of (a) 0.74 s, (b) 0.81 s, (c) 0.94 s, (d) 1.07 s, (e) 1.16 s, and (f) 1.32 s.

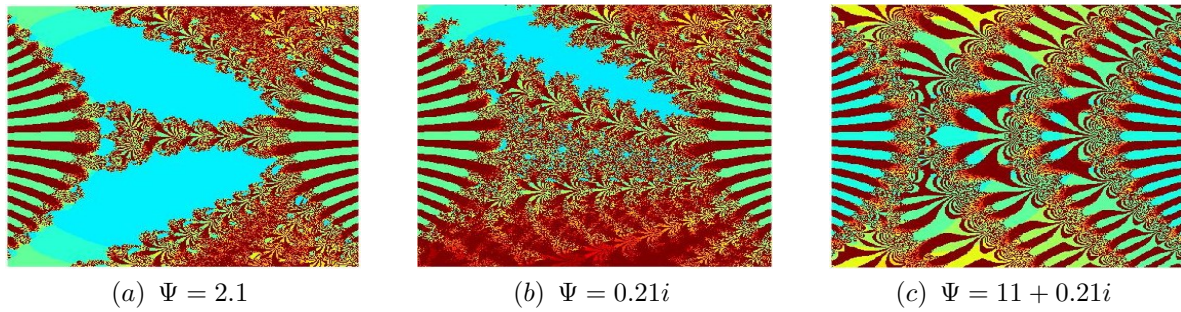


Figure 3. Julia sets generated for different  $\Psi$  values using Algorithm 1. The execution times for the images are: (a) 0.84 s, (b) 0.97 s, and (c) 1.17 s.

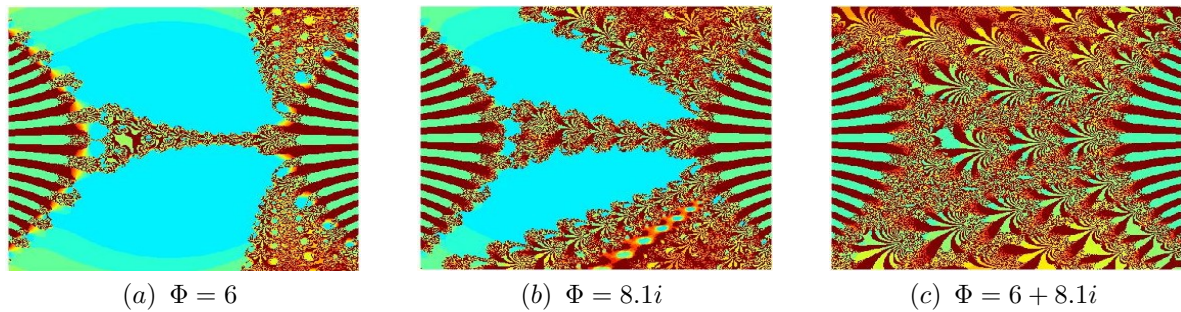


Figure 4. Julia sets generated for different  $\Phi$  values using Algorithm 1. The execution times for the images are: (a) 0.94 s, (b) 1.19 s, and (c) 1.38 s.

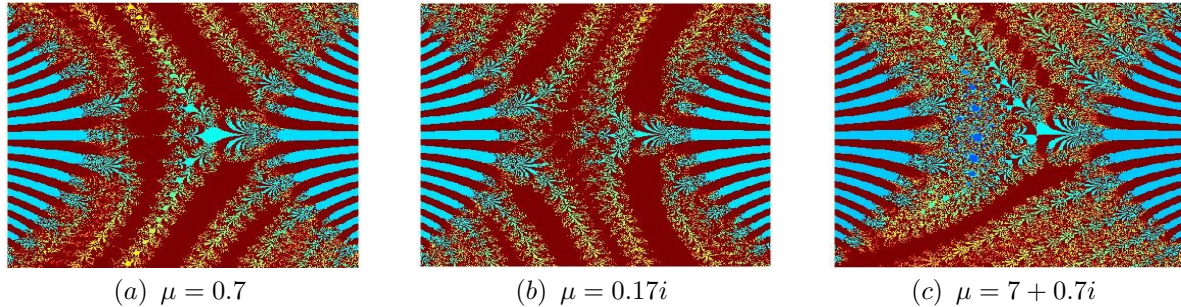


Figure 5. Julia sets generated for different  $\mu$  values using Algorithm 1. The execution times for the images are: (a) 1.09 s, (b) 1.22 s, and (c) 1.43 s.

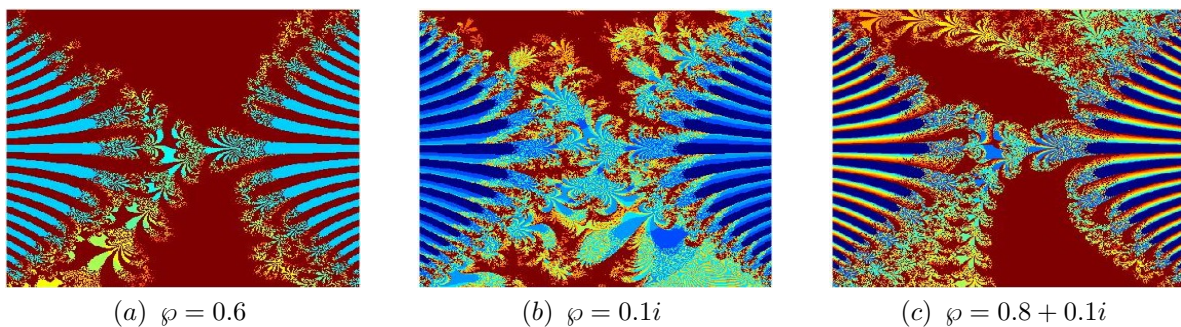


Figure 6. Julia sets generated for different  $\wp$  values using Algorithm 1. The execution times for the images are: (a) 1.13 s, (b) 1.28 s, and (c) 1.47 s.

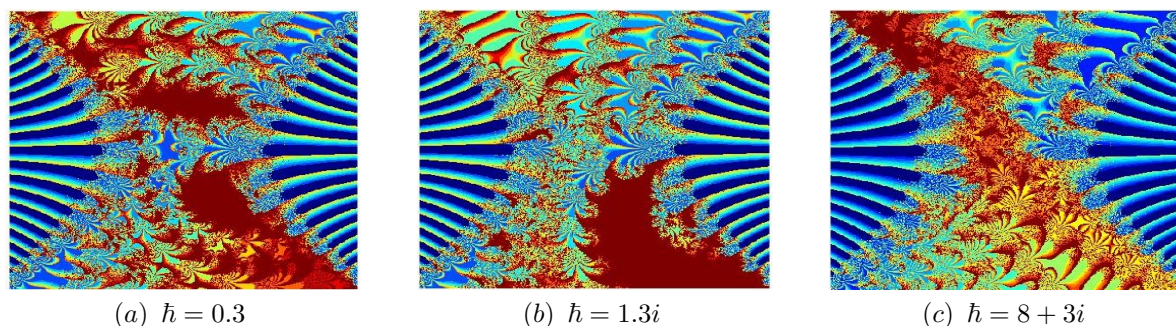


Figure 7. Julia sets generated for different  $\hbar$  values using Algorithm 1. The execution times for the images are: (a) 1.23 s, (b) 1.46 s, and (c) 1.68 s.

In second example, we investigate the influence of the parameters  $p, q, \omega, \eta$  and  $s$  to Julia sets for  $\mathcal{U}(z) = \Psi e^{z^p} + \frac{\Phi}{z^q} + \log \mu^\ell$  via (3.1) are generated here with the following inputs:  $\Psi = 0.21, \Phi = 0.11i, \mu = 0.8, \wp = 0.1i, \hbar = 0.3, \ell = 6$  and  $\varsigma = 0.5$ . The execution times for generating these images are also provided in seconds.

(i) In Fig. 8: Fixed parameters  $\omega = 0.09, \eta = 0.15, s = 0.21$ , and varied integer value of  $p$  and  $q$  as: (a)  $p = 2, q = 2$ , (b)  $p = 4, q = 2$ , (c)  $p = 8, q = 2$  (d)  $p = 2, q = 5$ , (e)  $p = 6, q = 7$ , (f)  $p = 6, q = 26$ .

(ii) In Fig. 9: Fixed parameters  $p = 4, q = 45, s = 0.85$ , and varied integer value of  $\omega$  and  $\eta$  as: (a)  $\omega = 0.17, \eta = 0.085$ , (b)  $\omega = 0.75, \eta = 0.085$ , (c)  $\omega = 0.075, \eta = 0.25$ , (d)  $\omega = 0.075, \eta = 0.85$ , (e)  $\omega = 0.25, \eta = 0.25$ , (f)  $\omega = 0.85, \eta = 0.85$ .

(iii) In Fig. 10: Fixed parameters  $p = 4, q = 4, \omega = 0.1, \eta = 0.2$ , and varied value of  $s$  as: (a)  $s = 0.15$ , (b)  $s = 0.55$ , (c)  $s = 0.95$ .

In Figures 8-10, we illustrate the impact of varying the parameters  $p, q, \omega, \eta$  and  $s$ , while keeping all other parameters fixed. As illustrated in Figure 8 (a-f) for even and odd values of  $p$  and  $q$ , the sets evolve into circular shapes with a number of petals determined by  $p$  and  $q$ ; this petal count increases as their values rise. Furthermore, the number of petals increases as  $p$  and  $q$  increase. Despite this, the patterns retain their fascinating rosette-like symmetry. These variations demonstrate that these parameters significantly influence the shape, size, and coloration of the sets, particularly near the edges of a leaf-like structure and rosette-shaped designs. Furthermore, we observe that as the values of  $p$  and  $q$  increase, the Julia sets generated become more complex, and the overall shape of the set undergoes notable changes. The changes in shape are non-uniform across the arms, yet the resulting sets maintain axial symmetry. Similarly, for parameters  $\omega$  and  $\eta$  (Figure 9), higher values produce more intricate leaf-shaped edges and elaborate rosette designs, with the petal count again escalating. While these changes can be non-uniform across the fractal arms, the resulting sets consistently maintain axial symmetry. Additionally, we observe that as the values of  $\omega$  and  $\eta$  increase, the generated Julia sets become more beautiful, with the overall shape of the set undergoing notable changes.

Furthermore, the influence of parameter  $s$  is detailed in Figure 10, where higher values are shown to produce decreasingly intricate leaf-shaped edges and more elaborate rosette designs, with the petal count escalating accordingly. Although these morphological changes can be non-uniform across the fractal's arms, the resulting sets consistently preserve their axial symmetry. The escalation in the value of  $s$  not only introduces notable alterations to the overall shape but also enhances the aesthetic complexity, yielding Julia sets of remarkable beauty. The final Julia sets exhibit remarkable complexity, bearing a visual resemblance to traditional Rangoli patterns, rosette-shaped designs, floral designs, or delicate glass artwork.

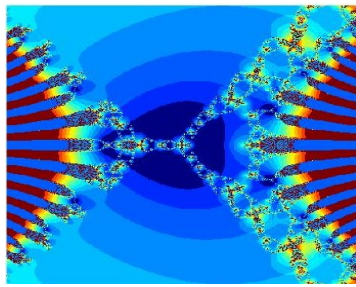
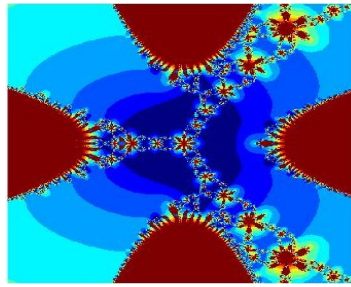
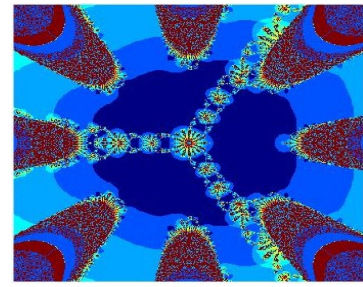
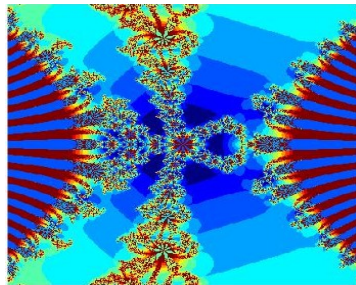
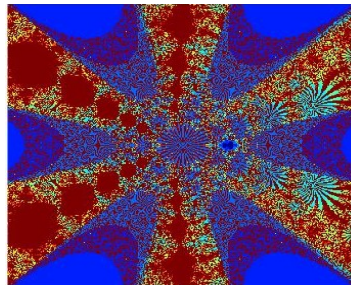
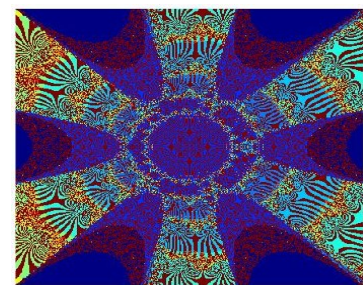
(a)  $p = 2$  and  $q = 2$ (b)  $p = 4$  and  $q = 2$ (c)  $p = 8$  and  $q = 2$ (d)  $p = 2$  and  $q = 5$ (e)  $p = 6$  and  $q = 7$ (f)  $p = 6$  and  $q = 26$ 

Figure 8. Julia sets generated for different  $p$  and  $q$  values using Algorithm 1. The execution times for the images are: (a) 1.24 s, (b) 1.41 s, (c) 1.54 s, (d) 1.67 s, (e) 1.84 s, and (f) 2.03 s.

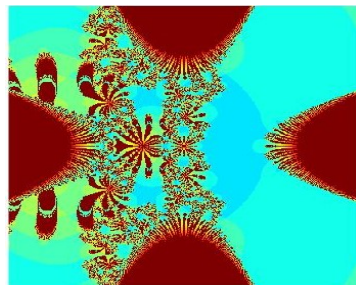
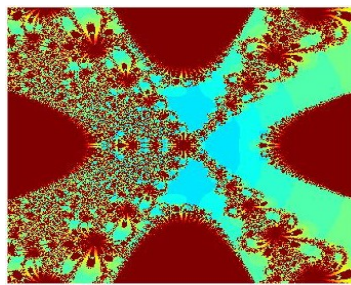
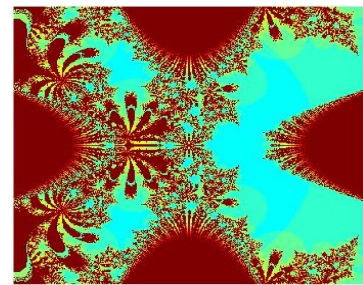
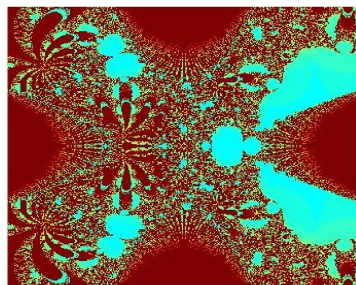
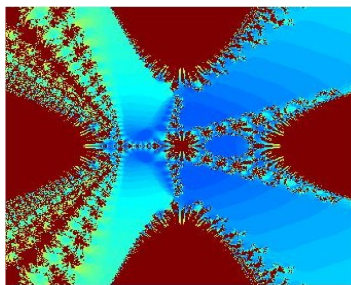
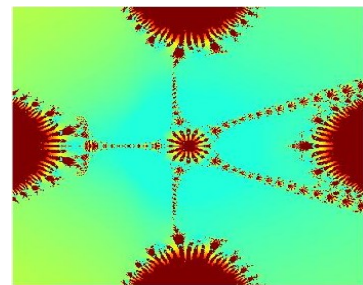
(a)  $\omega = 0.17$  and  $\eta = 0.085$ (b)  $\omega = 0.75$  and  $\eta = 0.085$ (c)  $\omega = 0.075$  and  $\eta = 0.25$ (d)  $\omega = 0.075$  and  $\eta = 0.85$ (e)  $\omega = 0.25$  and  $\eta = 0.25$ (f)  $\omega = 0.85$  and  $\eta = 0.85$ 

Figure 9. Julia sets generated for different  $\omega$  and  $\eta$  values using Algorithm 1. The execution times for the images are: (a) 1.51 s, (b) 1.76 s, (c) 1.97 s, (d) 2.23 s, (e) 2.41 s, and (f) 2.71 s.

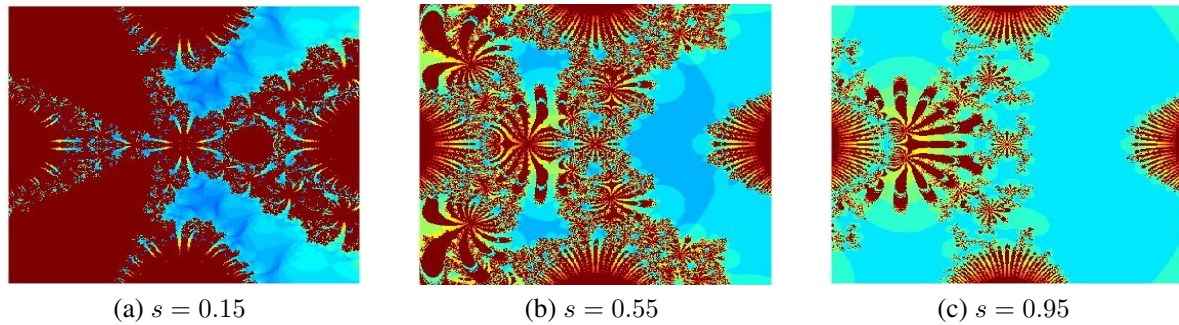


Figure 10. Julia sets generated for different  $s$  values using Algorithm 1. The execution times for the images are: (a) 2.14 s, (b) 2.37 s, and (c) 2.53 s.

In third example, we investigate the influence of the parameters  $\ell, \Psi, \Phi, p, q, \omega, \eta$  and  $s$  to Mandelbrot sets for  $\mathcal{U}(z) = \Psi e^{z^p} + \frac{\Phi}{z^q} + \log \mu^\ell$  via (3.1) are generated here with the following inputs:  $\wp = 0.8i, \hbar = 0.41, \varsigma = 0.25$  and  $K = 70$ . The image generation time for each iteration is also recorded.

- (i) In Fig. 11: Fixed parameters  $p = 2, q = 2, \Psi = 31, \Phi = 0.4, \omega = 0.7, \eta = 0.8, s = 0.71$ , and varied the value of  $\ell$  as: (a)  $\ell = 2$ , (b)  $\ell = 6$ , (c)  $\ell = 13.5$ .
- (ii) In Fig. 12: Fixed parameters  $p = 2, q = 2, \ell = 2, \Phi = 0.4, \omega = 0.7, \eta = 0.8, s = 0.71$ , and varied integer value of  $\Psi$  as: (a)  $\Psi = 0.31$ , (b)  $\Psi = 0.31i$ , (c)  $\Psi = 0.1 + 0.31i$ .
- (iii) In Fig. 13: Fixed parameters  $p = 2, q = 2, \ell = 2, \Psi = 0.31, \omega = 0.7, \eta = 0.8, s = 0.71$ , and varied integer value of  $\Psi$  as: (a)  $\Psi = 0.21$ , (b)  $\Psi = 0.21i$ , (c)  $\Psi = 0.3 + 0.21i$ .
- (iv) In Fig. 14: Fixed parameters  $\ell = 2, \Psi = 0.31, \Psi = 0.2, \omega = 0.7, \eta = 0.8, s = 0.71$ , and varied integer value of  $p$  and  $q$  as: (a)  $p = 2, q = 2$  (b)  $p = 6, q = 6$  (c)  $p = 6, q = 3$ .
- (v) In Fig. 15: Fixed parameters  $\ell = 2, p = 6, q = 2, \Psi = 0.31, \Psi = 0.2, s = 0.71$ , and varied integer value of  $\omega$  and  $\eta$  as: (a)  $\omega = 0.1, \eta = 3$  (b)  $\omega = 0.5, q = 0.4$  (c)  $\omega = 0.8, q = 0.9$ .
- (vi) In Fig. 16: Fixed parameters  $\ell = 2, p = 6, q = 2, \Psi = 0.31, \Psi = 0.2, \omega = 0.7, \eta = 0.9$ , and varied integer value of  $s$  as: (a)  $s = 0.25$  (b)  $s = 0.65$  (c)  $s = 0.95$ .

In Figures 11-16 (a, b, c), display Mandelbrot sets generated by fixing one parameter either  $\ell, \Psi, \Phi, p, q, \omega, \eta$  or  $s$  while varying the others. In 12-13(a, b, c),  $\Psi$  and  $\Phi$  are assigned purely real values in (a) purely imaginary in (b), and complex in (c). Furthermore, Figures 11 and 14-16 (a, b, c) reveal that as  $\ell, p, q, \omega, \eta$  and  $s$  increase, the sets transform into circular structures, with petal counts determined by  $p, q$  and  $s$ . These variations highlight the critical influence of  $\ell, \Psi, \Phi, p, q, \omega, \eta$  or  $s$  on the shape, size, and coloration of the sets, particularly near the leaf-like edges.

While the shape changes non-uniformly across the arms, the resulting sets maintain axial symmetry. Moreover, the number of petals grows with increasing parameter values. Although the transformations often proceed non-uniformly across the fractal's arms, a consistent axial symmetry is preserved throughout. The culminating Mandelbrot sets display remarkable and striking complexity, their forms bearing a strong visual resemblance to intricate Rangoli patterns, elaborate floral motifs, or delicate glass art. The image generation time for each iteration is also recorded.

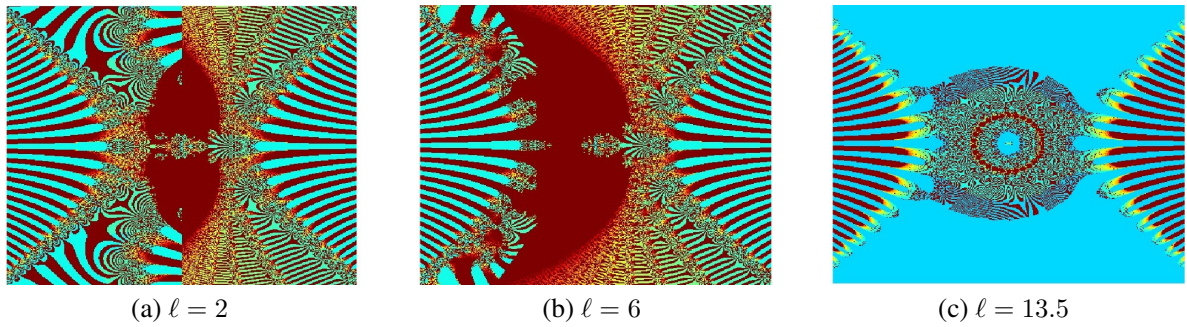


Figure 11. Mandelbrot sets generated for different  $\ell$  values using Algorithm 2. The execution times for the images are: (a) 1.54 s, (b) 1.76 s, and (c) 1.91 s.

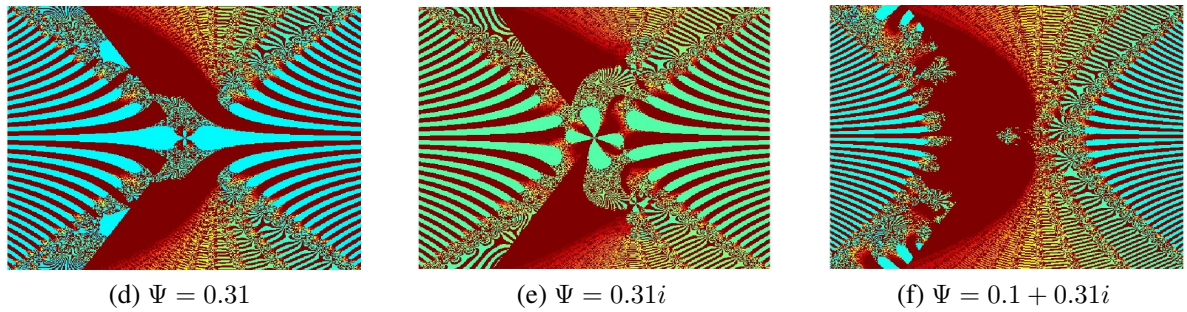


Figure 12. Mandelbrot sets generated for different  $\Psi$  values using Algorithm 2. The execution times for the images are: (a) 1.61 s, (b) 1.83 s, and (c) 1.96 s.

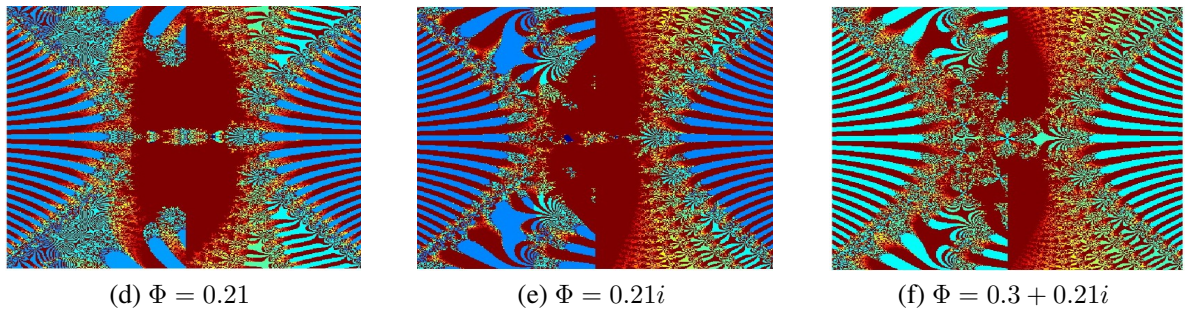


Figure 13. Mandelbrot sets generated for different  $\Phi$  values using Algorithm 2. The execution times for the images are: (a) 1.68 s, (b) 1.81 s, and (c) 1.98 s.

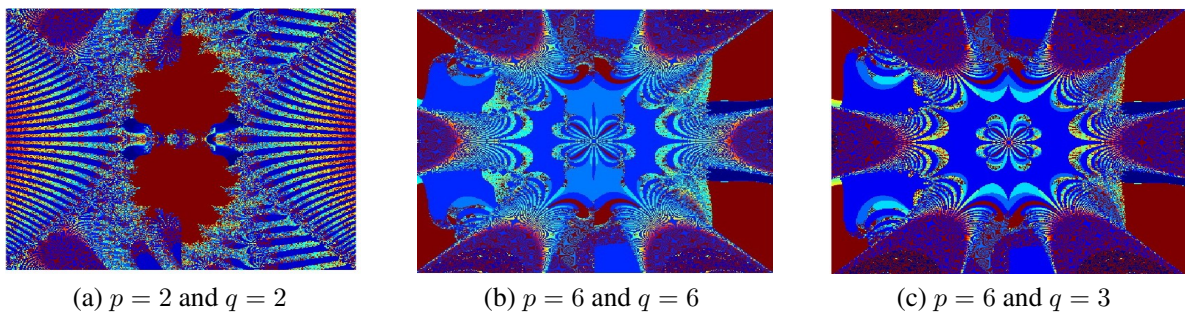


Figure 14. Mandelbrot sets generated for different  $p$  and  $q$  values using Algorithm 2. The execution times for the images are: (a) 1.74 s, (b) 1.94 s, and (c) 2.14 s.

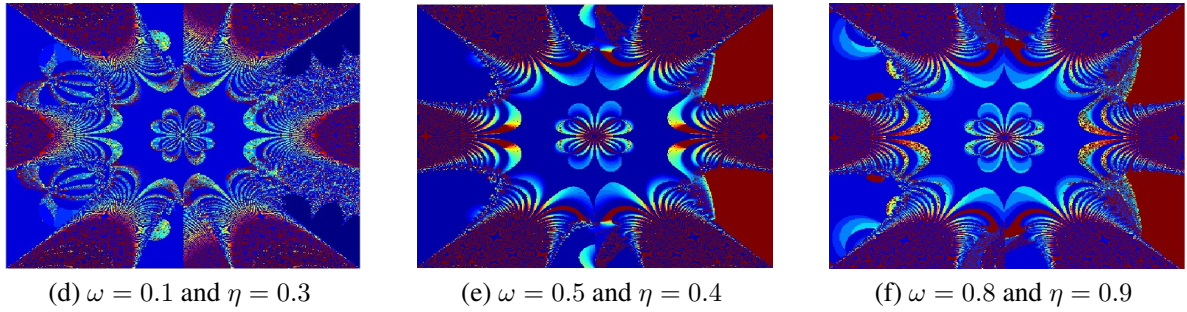


Figure 15. Mandelbrot sets generated for different  $\omega$  and  $\eta$  values using Algorithm 2. The execution times for the images are: (a) 1.83 s, (b) 2.08 s, and (c) 2.27 s.

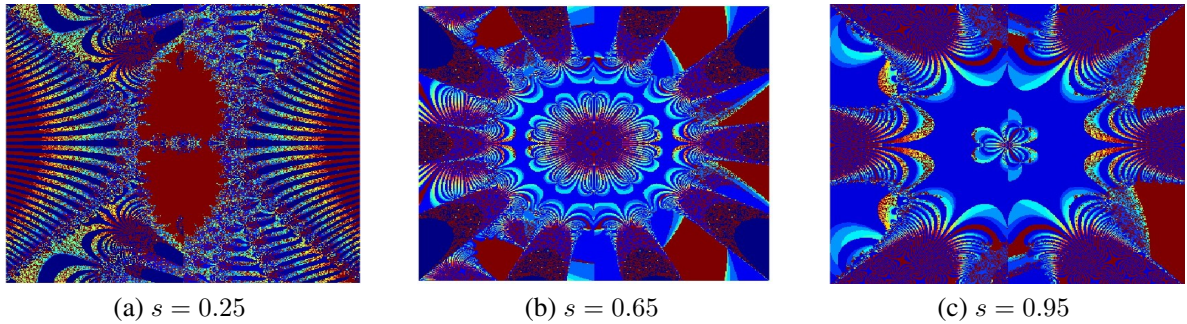


Figure 16. Mandelbrot sets generated for different  $s$  values using Algorithm 2. The execution times for the images are: (a) 2.04 s, (b) 2.26 s, and (c) 2.48 s.

**4.2. Julia and Mandelbrot sets generation for  $\mathcal{V}(z) = \Psi \cos(z^p) + \frac{\Phi}{z^q} + \log \mu^\ell$**

This subsection presents the Julia and Mandelbrot sets corresponding to (2.2) for various input values.

---

**Algorithm 3** Julia set generation for  $\mathcal{V}(z) = \Psi \cos(z^p) + \frac{\Phi}{z^q} + \log \mu^\ell$

---

**Input:**  $\mathcal{V}(z) = \Psi \cos(z^p) + \frac{\Phi}{z^q} + \log \mu^\ell$ , where  $p \geq 2, p, q \in \mathbb{N}, \Psi, \Phi \in \mathbb{C}, \mu \in \mathbb{C} \setminus \{0\}, \ell \geq 1$ .  
 $A \subset \mathbb{C}$ -area in which we draw the set;  $K$ -maximal number of iterations;  $\omega, \eta \in (0, 1)$ ;  
 $\mathcal{J}(z) = \wp z + \hbar$ , where  $\wp, \hbar \in \mathbb{C}$  with  $|\wp| < 1$ ; colourmap  $[0..C-1]$ -color with  $C$  colors.

**Output:** Julia set for area  $A$

**for**  $z_0 \in A$  **do**  
 $\tau = \frac{\log(\mu^\ell)}{\mu}$   
 $R' = \max \left\{ |\mu|, |\hbar|, \left| \Phi^{\frac{1}{p+q}} \right|, \left( \frac{(2+s\omega|\wp|+(1-s\omega)(1-s\eta)|\tau|)}{(1-s\eta)(1-s\omega)(|\Psi||\xi|-1)} \right)^{\frac{1}{p-1}} \right\}$ ,  
 $j = 0$   
**while**  $j \leq K$  **do**  
 $z_{j+1} = \omega^s \mathcal{J}(z_j) + (1 - \omega)^s \vartheta_j$ ,  
 $\vartheta_j = \eta^s z_j + (1 - \eta)^s \mathcal{U}(z_j)$ , where  $0 < \omega, \eta < 1$   
**if**  $|z_{j+1}| \geq R'$  **then break end if**  $j = j + 1$   
 colour  $z_0$  with colourmap  $[J]$

---

---

**Algorithm 4** Mandelbrot set generation for  $\mathcal{V}(z) = \Psi \cos(z^p) + \frac{\Phi}{z^q} + \log \mu^\ell$

---

**Input:**  $\mathcal{V}(z) = \Psi \cos(z^p) + \frac{\Phi}{z^q} + \log \mu^\ell$ , where  $p \geq 2, q \in \mathbb{N}, \Psi, \Phi \in \mathbb{C}, \mu \in \mathbb{C} \setminus \{0\}, \ell \geq 1$ .  
 $A \subset \mathbb{C}$ -area in which we draw the set;  $K$ -maximal number of iterations;  $\omega, \eta \in (0, 1)$ ;  
 $\mathcal{J}(z) = \wp z + \hbar$ , where  $\wp, \hbar \in \mathbb{C}$  with  $|\wp| < 1$ ; colourmap  $[0..C-1]$ -color with  $C$  colors.

**Output:** Mandelbrot set for area  $A$

**for**  $z_0 \in A$  **do**  
 $\tau = \frac{\log(\mu^\ell)}{\mu}$  and  
 $R' = \max \left\{ |\mu|, |\hbar|, \left| \Phi \frac{1}{p+q} \right|, \left( \frac{(2+s\omega|\wp|+(1-s\omega)(1-s\eta)|\tau|)}{(1-s\eta)(1-s\omega)(|\Psi||\xi|-1)} \right)^{\frac{1}{p-1}} \right\}$ ,  
 $j = 0$   
 $z_0 = \mu$   
**while**  $j \leq K$  **do**  
 $z_{j+1} = \omega^s \mathcal{J}(z_j) + (1 - \omega^s) \vartheta_j$ ,  
 $\vartheta_j = \eta^s z_j + (1 - \eta)^s \mathcal{U}(z_j)$ , where  $0 < \omega, \eta < 1$  and  $0 < s \leq 1$   
**if**  $|z_{j+1}| \geq R'$  **then break end if**  $j = j + 1$   
**colour**  $z_0$  **with colourmap**  $[J]$

---

In this example, we explore two scenarios: one with integer values of  $\ell$  and another with non-integer value of  $\ell$ . Using (3.1), we generate Julia sets  $\mathcal{V}(z) = \Psi \cos(z^p) + \frac{\Phi}{z^q} + \log \mu^\ell$  under the following parameter choices:

- (i) In Fig. 17: Fixed parameters  $p = 2, q = 1, \Psi = 3 + 0.82i, \Phi = 0.11 + 5i, \mu = 0.3 + 2i, \omega = 0.2, \eta = 0.4, \xi = 0.2, \wp = 0.6, \hbar = 1.3, s = 0.71$ , and varied integer value of  $\ell$  as: (a) 3, (b) 8, (c) 32, (d) 1.2, (e) 6.4, (f) 18.6.
- (ii) In Fig. 18: Fixed parameters  $p = 2, q = 1, \ell = 2, \Phi = 0.11 + 5i, \mu = 0.3 + 2i, \wp = 0.8, \hbar = 0.3, \omega = 0.15, \eta = 0.25, \xi = 0.2, \wp = 0.6, \hbar = 1.3, s = 0.71$ , and varied  $\Psi$  as: (a) 0.11, (b) 0.82i, (c) 0.11 + 0.22i.
- (iii) In Fig. 19: Fixed parameters  $p = 2, q = 1, \Psi = 0.21, \mu = 0.2, \wp = 0.6, \hbar = 1.53, \xi = 0.2, \omega = 0.15, \eta = 0.5, s = 0.45, \ell = 2$ , and varied  $\Phi$  as: (a) 0.1, (b) 0.31i, (c) 0.16 + 0.015i.
- (iv) In Fig. 20: Fixed parameters  $p = 2, q = 1, \Psi = 0.16i, \Phi = 0.016 + 0.014i, \wp = 0.6, \hbar = 1.53, \xi = 0.2, \omega = 0.15, \eta = 0.3, s = 0.85, \ell = 2$ , and varied  $\mu$  as: (a) 0.6, (b) 0.31i, (c) 0.14 + 0.12i.
- (v) In Fig. 21: Fixed parameters  $p = 2, q = 1, \Phi = 0.21, \Psi = 0.11, \mu = 0.4, \hbar = 1.53, \xi = 0.2, \omega = 0.2, \eta = 0.4, s = 0.45, \ell = 2$ , and varied  $\wp$  as: (a) 0.6, (b) 0.6i, (c) 0.6 + 0.4i.
- (vi) In Fig. 22: Fixed parameters  $p = 2, q = 1, \Phi = 0.1, \Psi = 0.21, \mu = 0.5, \wp = 0.56, \xi = 0.2, \omega = 0.2, \eta = 0.4, s = 0.71, \ell = 2$ , and varied  $\hbar$  as: (a) 1.53, (b) 0.003i, (c) 0.3 + 0.2i.

The generation and morphological evolution of Julia sets under a controlled parameter space are systematically illustrated in Figures 17-22 (a, b, c), which explore the influence of the parameters  $\ell, \Psi, \Phi, \omega, \eta, \wp, \hbar$  and  $s$ . An initial, detailed examination in Figure 17 establishes the critical role of parameter sub-figures  $\ell$ : (a) - (c) display integer values  $\ell$ , while (d) - (f) show non-integer cases, this comparison reveals that even minor variations in  $\ell$  can induce dramatically different structural patterns, highlighting its sensitivity. Subsequent analysis in Figures 18-22 further dissects the impact of other parameters by employing a consistent tripartite framework: sub-figure (a) for purely real values, (b) for purely imaginary values, and (c) for complex values. These variations clearly demonstrate how  $\Psi, \Phi, \mu, \wp$ , and  $\hbar$  govern the geometric patters, leaf-like formations, where the edge structures exhibit a consistent and intricate fourfold symmetry. A particularly intriguing outcome of these parametric manipulations is the emergence of biomorphic forms, with certain fractal configurations exhibiting a striking resemblance to like ants, as evidenced in Figure 19(a), and Figure 20(a). The culmination of this exploration is a series of patterns of remarkable complexity and aesthetic refinement, whose intricate forms bear a visual resemblance to a fascinating spectrum of natural and artistic motifs—from the ant-like shapes to traditional Rangoli art, elaborate floral designs, and the delicate, colorful patterns of stained glasswork. For reference, the computational image generation time for each iterative process was also recorded.

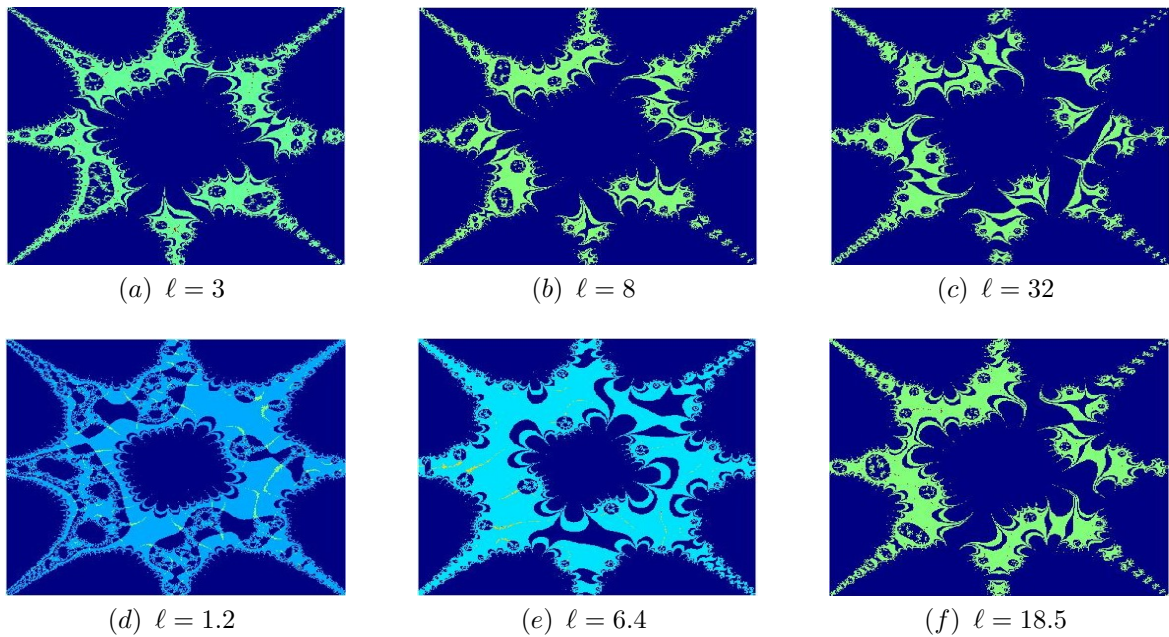


Figure 17. Julia sets generated for different  $\ell$  values using Algorithm 3. The execution times for the images are: (a) 0.84 s, (b) 1.02 s, (c) 1.18 s, (d) 1.36 s, (e) 1.43 s, and (f) 1.61 s.

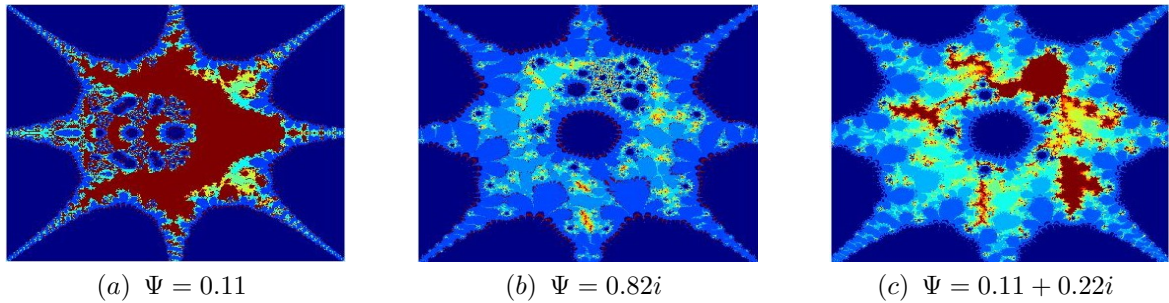


Figure 18. Julia sets generated for different  $\Psi$  values using Algorithm 3. The execution times for the images are: (a) 1.23 s, (b) 1.51 s, and (c) 1.73 s.

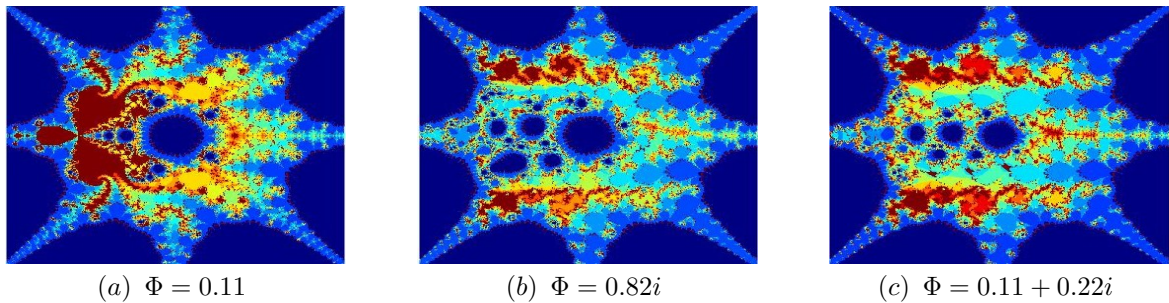


Figure 19. Julia sets generated for different  $\Phi$  values using Algorithm 3. The execution times for the images are: (a) 1.21 s, (b) 1.47 s, and (c) 1.61 s.

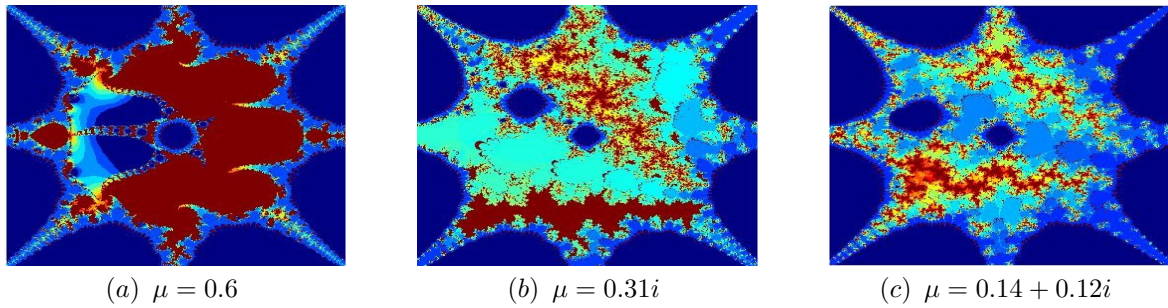


Figure 20. Julia sets generated for different  $\mu$  values using Algorithm 3. The execution times for the images are: (a) 1.41 s, (b) 1.57 s, and (c) 1.68 s.

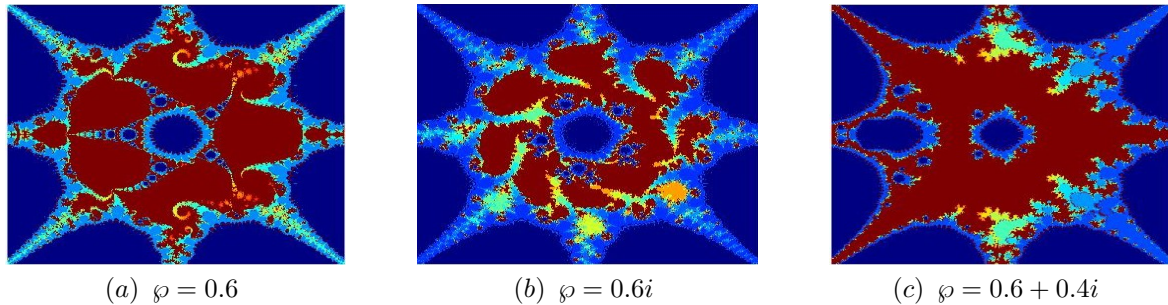


Figure 21. Julia sets for different values of  $\varphi$  generated via Algorithm 3. The execution times for the images are: (a) 1.55 s, (b) 1.76 s, and (c) 1.88 s.

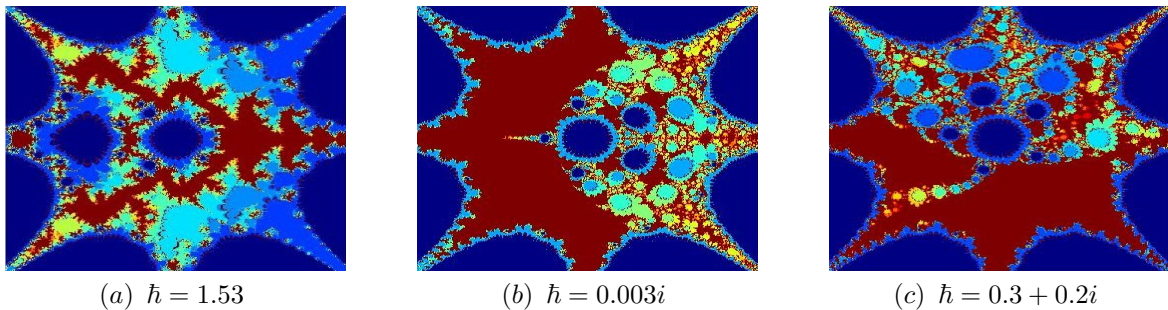


Figure 22. Julia sets for different values of  $\hbar$  generated via Algorithm 3. The execution times for the images are: (a) 1.61 s, (b) 1.82 s, and (c) 1.97 s.

In this second example, we examine the effect of parameters  $p, q, \omega, \eta,$  and  $s$  to generate the Julia sets for  $\mathcal{V}(z) = \Psi \cos(z^p) + \frac{\Phi}{z^q} + \log \mu^\ell$  using (3.1), with the following parameter configurations:  $\ell = 2, \Psi = 0.1 - 0.5i, \Phi = 35i, \mu = 0.4, \varphi = 0.15$  and  $\hbar = 0.31 + 0.23i$ .

- (i) In Fig. 23: Fixed parameters  $\omega = 0.15, \eta = 0.5, s = 0.71,$  and varied integer value of  $p$  and  $q$  as: (a)  $p = 2, q = 1,$  (b)  $p = 4, q = 1,$  (c)  $p = 8, q = 2$  (d)  $p = 2, q = 4,$  (e)  $p = 2, q = 9,$  (f)  $p = 10, q = 10.$
- (ii) In Fig. 24: Fixed parameters  $p = 2, q = 2, s = 0.5,$  and varied integer value of  $\omega$  and  $\eta$  as: (a)  $\omega = 0.95, \eta = 0.0003,$  (b)  $\omega = 0.95, \eta = 0.015,$  (c)  $\omega = 0.95, \eta = 0.85,$  (d)  $\omega = 0.0015, \eta = 0.75,$  (e)  $\omega = 0.4, \eta = 0.5,$  (f)  $\omega = 0.6, \eta = 0.6.$
- (iii) In Fig. 25: Fixed parameters  $p = 4, q = 4, \omega = 0.1, \eta = 0.2,$  and varied value of  $s$  as: (a)  $s = 0.15,$  (b)  $s = 0.55,$  (c)  $s = 0.95.$

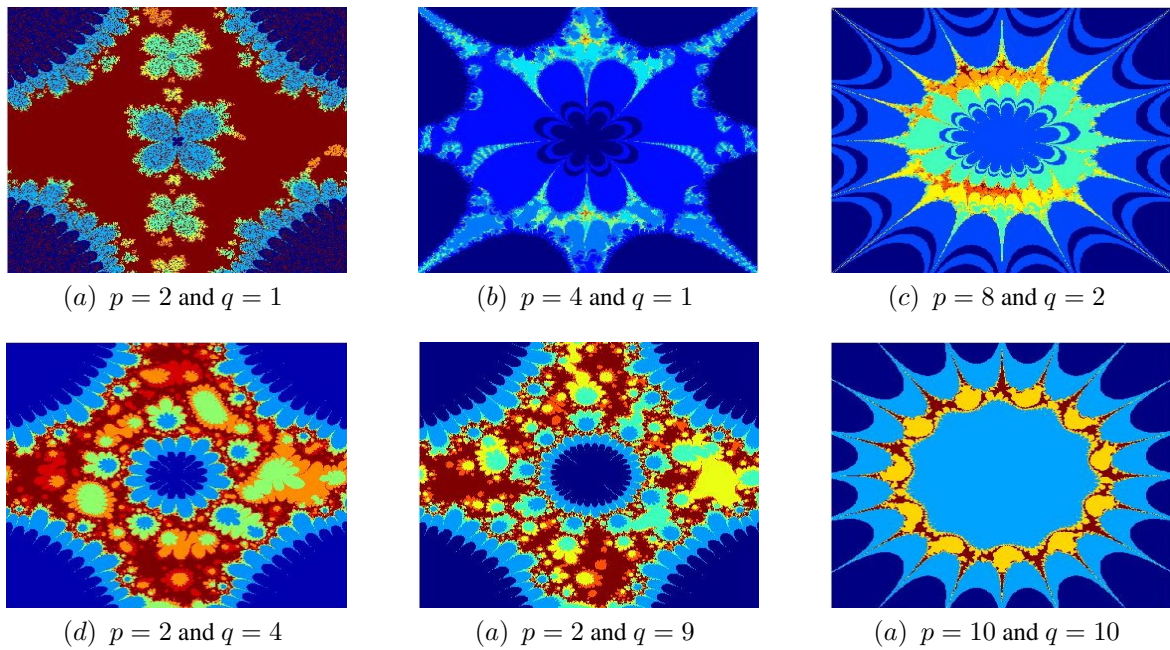


Figure 23. Julia sets generated for different  $p$  and  $q$  values using Algorithm 3. The execution times for the images are: (a) 0.84 s, (b) 1.02 s, (c) 1.18 s, (d) 1.36 s, (e) 1.43 s, and (f) 1.61 s.

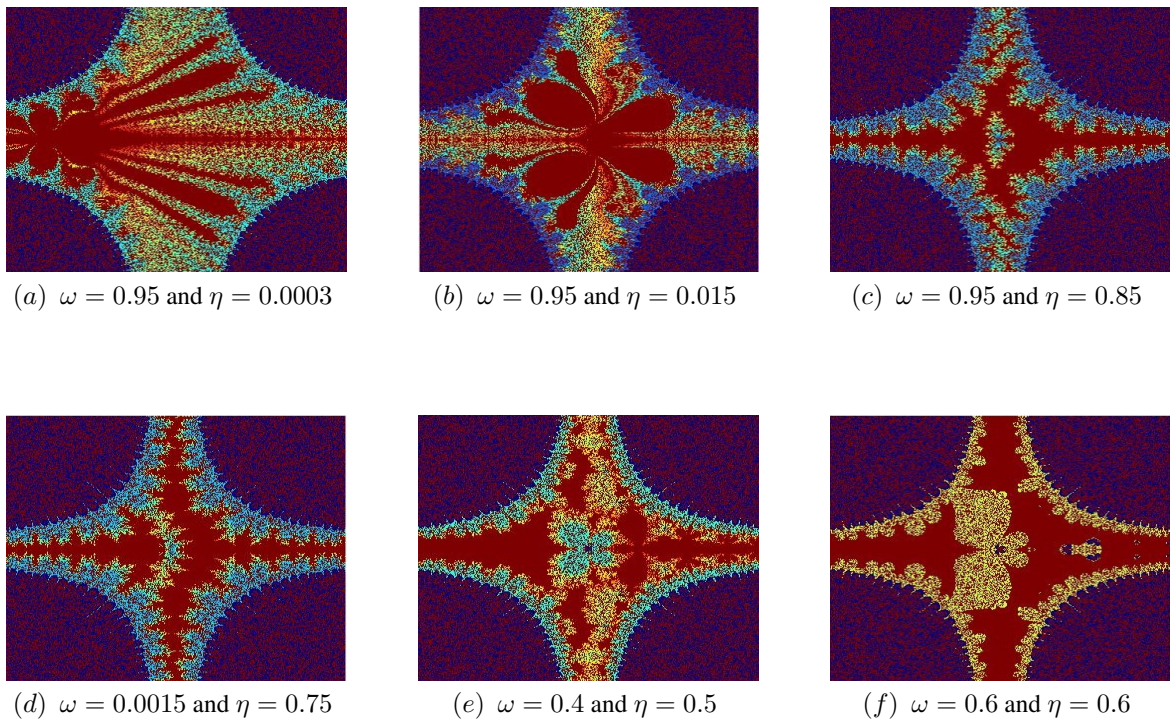


Figure 24. Julia sets generated for different  $\omega$  and  $\eta$  values using Algorithm 3. The execution times for the images are: (a) 1.44 s, (b) 1.62 s, (c) 1.87 s, (d) 1.94 s, (e) 2.23 s, and (f) 2.51 s.

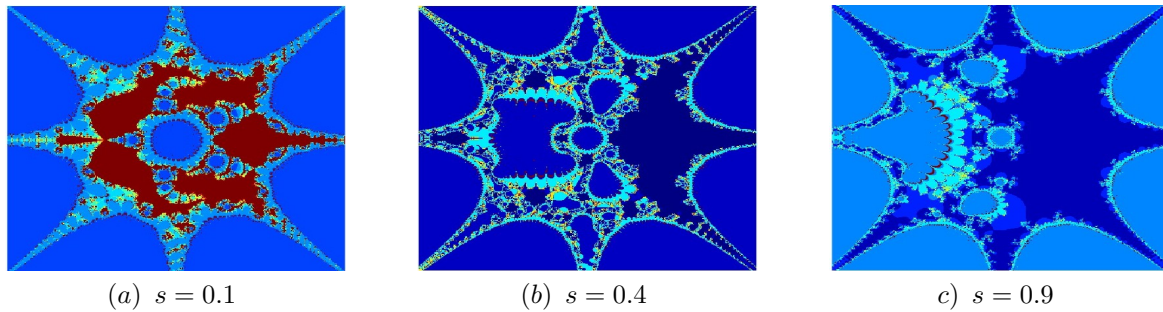


Figure 25. Julia sets generated for different  $s$  values using Algorithm 3. The execution times for the images are: (a) 1.91 s, (b) 2.22 s, and (c) 2.47 s.

Figures 23-25 illustrate the influence of the parameters  $p, q, \omega, \eta$  and  $s$  shape Julia sets generated via Algorithm 3 for  $\mathcal{V}(z)$ . These variations highlight the critical influence of  $p, q, \omega, \eta$  and  $s$  on the shape, size, and coloration of the sets, particularly near the leaf-like edges. While the shape changes non-uniformly across the arms, the resulting sets maintain axial symmetry. Moreover, the number of petals grows with increasing parameter values. The resulting Julia sets exhibit striking complexity, resembling intricate Rangoli patterns, floral motifs, or delicate glass art. Notably, certain parameter combinations yield fractals with a distinct biomorphic appearance, closely resembling ants (see Figure 24(a-c)). Furthermore, a key dynamical transition is observed: as the values of  $\omega$  and  $\eta$  increase, the set loses its connectivity and disintegrates into a dust-like collection of points (see Figure 24(c-f)). The culmination of these parametric manipulations is a gallery of patterns exhibiting remarkable complexity, whose forms range from ant-like shapes to intricate designs reminiscent of traditional Rangoli art, floral motifs, and delicate stained glasswork. Finally, all the presented fractals demonstrate remarkable innovation and aesthetic appeal, arising from the sophisticated interplay between the function  $\mathcal{V}(z)$ .

In this final example, we examine the specific influence of the parameters  $p, q, \ell, \Psi, \Phi, \omega, \eta$  and  $s$  on the generation of Mandelbrot sets for the complex map  $\mathcal{V}(z) = \Psi \cos(z^p) + \frac{\Phi}{z^q} + \log \mu^\ell$  using Algorithm 4, with the following parameter configurations:  $\wp = 0.2, \hbar = 0.3$  and  $\xi = 0.2$ .

- (i) In Fig. 26: Fixed parameters  $p = 3, q = 3, \Psi = 0.031, \Phi = 0.2, \omega = 0.0004, \eta = 0.25, s = 0.08$ , and varied value of  $\ell$  as: (a)  $\ell = 2$ , (b)  $\ell = 6$ , (c)  $\ell = 11.5$ .
- (ii) In Fig. 27: Fixed parameters  $p = 3, q = 3, \ell = 4, \Phi = 0.2, \omega = 0.0004, \eta = 0.25, s = 0.08$ , and varied value of  $\Psi$  as: (a)  $\Psi = 0.07$ , (b)  $\Psi = 0.003i$ , (c)  $\Psi = 0.07 + 0.003i$ .
- (iii) In Fig. 28: Fixed parameters  $p = 3, q = 3, \ell = 8, \Psi = 0.07 + 0.003i, \omega = 0.0004, \eta = 0.25, s = 0.08$ , and varied value of  $\Phi$  as: (a)  $\Phi = 0.02$ , (b)  $\Phi = 0.02i$ , (c)  $\Phi = 0.1 + 0.002i$ .
- (iv) In Fig. 29: Fixed parameters  $\ell = 8, \Psi = 0.07 + 0.003i, \Phi = 0.2, \omega = 0.01, \eta = 0.7, s = 0.08$ , and varied value of  $p$  and  $q$  as: (a)  $p = 3, q = 2$ , (b)  $p = 5, q = 5$ , (c)  $p = 4, q = 8$ .
- (v) In Fig. 30: Fixed parameters  $p = 4, q = 4, \ell = 8, \Psi = 0.31, \Phi = 0.2$ , and varied value of  $\omega$  and  $\eta$  as: (a)  $\omega = 0.0005, \eta = 0.25$ , (b)  $\omega = 0.004, \eta = 0.5$ , (c)  $\omega = 0.04, \eta = 0.85$ .
- (vi) In Fig. 31: Fixed parameters  $p = 4, q = 4, \ell = 8, \Psi = 0.31, \Phi = 0.2$ , and varied value of  $s$  as: (a)  $s = 0.1$ , (b)  $s = 0.3$ , (c)  $s = 0.6$ .

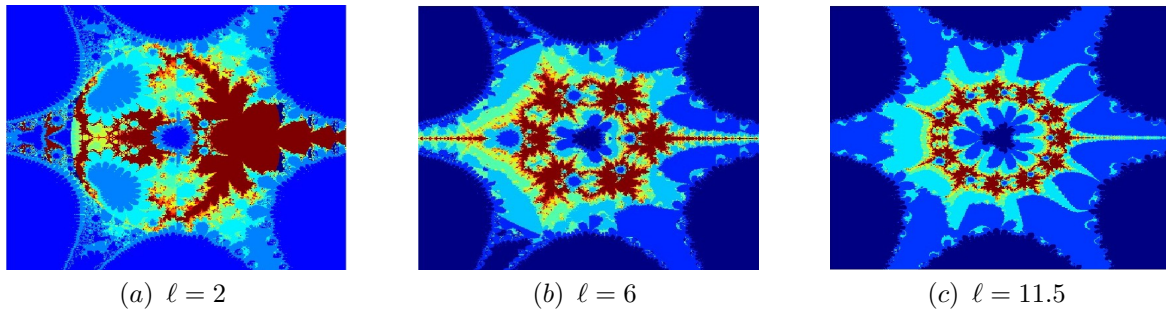


Figure 26. Mandelbrot sets generated via Algorithm 4 for different value of  $\ell$ . The execution times for the images are: (a) 1.53 s, (b) 1.82 s, and (c) 2.07 s.

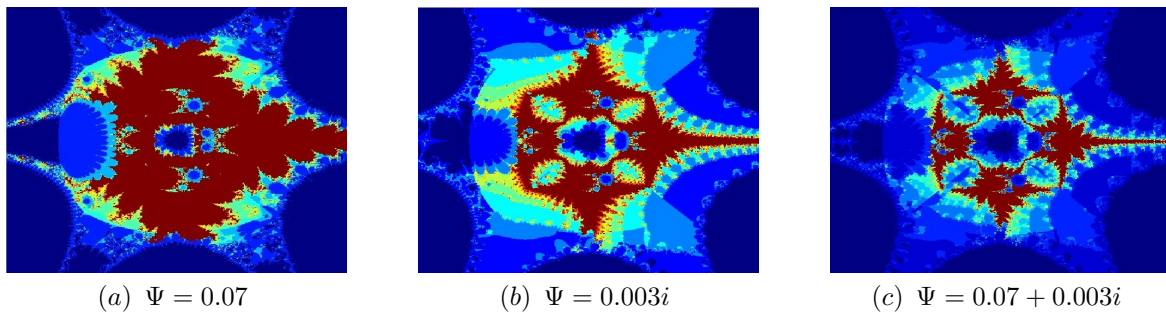


Figure 27. Mandelbrot sets generated via Algorithm 4 for different value of  $\Psi$ . The execution times for the images are: (a) 1.21 s, (b) 1.52 s, and (c) 1.87 s.

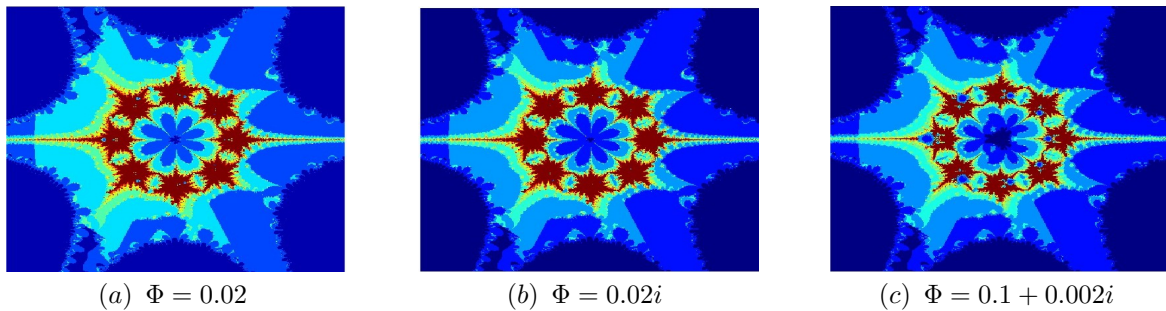


Figure 28. Mandelbrot sets generated via Algorithm 4 for different value of  $\Phi$ . The execution times for the images are: (a) 0.91 s, (b) 1.22 s, and (c) 1.67 s.

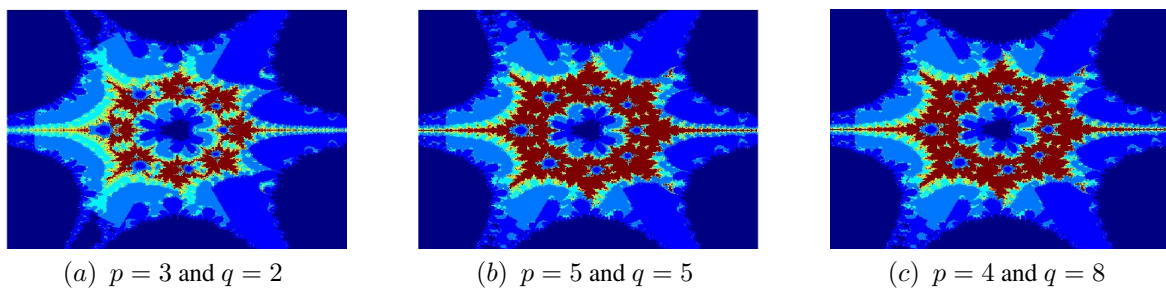


Figure 29. Mandelbrot sets generated via Algorithm 4 for different values of  $p$  and  $q$ . The execution times for the images are: (a) 2.11 s, (b) 2.32 s, and (c) 2.66 s.

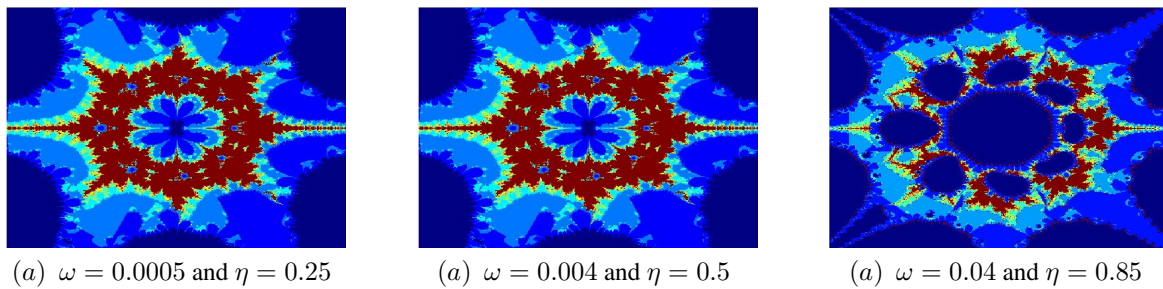


Figure 30. Mandelbrot sets generated via Algorithm 4 for different values of  $\omega$  and  $\eta$ . The execution times for the images are: (a) 2.49 s, (b) 2.69 s, and (c) 2.87 s.

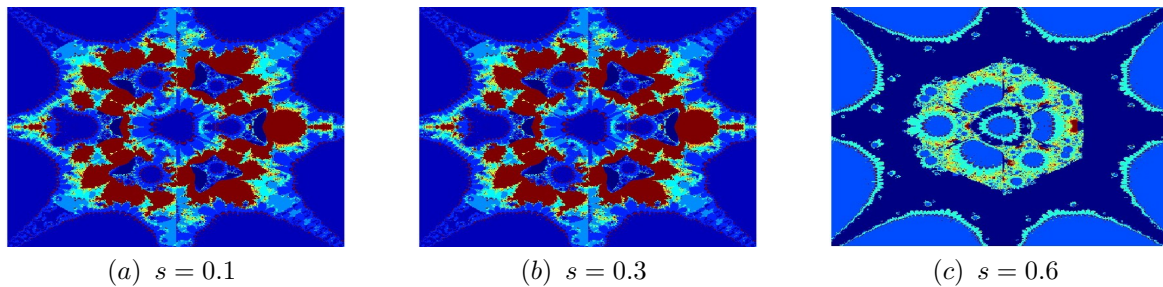


Figure 31. Mandelbrot sets generated via Algorithm 2 for different value of  $s$ . The execution times for the images are: (a) 2.88 s, (b) 3.08 s, and (c) 3.37 s.

The profound impact of parameters  $p, q, \ell, \Psi, \Phi, \omega, \eta$ , and  $s$  on the morphology of Mandelbrot sets is systematically demonstrated in Figures 26–31. As the values of these parameters  $p, q, \ell, \omega, \eta$ , and  $s$  increase, they induce substantial alterations to the geometric structure and scale of the sets, as visible in Figures 26, 29–31. This evolution is characterized by a marked increase in the complexity of the central morphology and the development of intricate peripheral patterns that evoke visual analogues such as floral arrangements, swirling motifs, multicolored teething rings, circular saw blades, and stained-glass artwork, all while maintaining distinct Mandelbrot point distributions. The resulting visual complexity and aesthetic refinement intensify with parameter variation, yielding progressively more elaborate fractal designs. Furthermore, the developed fractals exhibit notable novelty and aesthetic appeal, arising from the sophisticated mathematical properties of the complex functions  $\mathcal{U}(z)$  and  $\mathcal{V}(z)$ . These functions generate visually striking patterns that maintain both mathematical integrity and artistic beauty.

As the different value of the parameters  $p, q, \ell, \Psi, \Phi, \omega, \eta$ , and  $s$ , we notice that the value of the parameters have a great impact on the shape of the Julia set and its size. Moreover, the resulting sets display a remarkable variety of forms; some configurations yield patterns reminiscent of flowers, ants, or intricate rosette-shaped designs, while others bear a visual similarity to delicate glass paintings, albeit with the distinct mathematical underpinnings of Julia and Mandelbrot point distributions. Furthermore, varying these parameters introduces enhanced aesthetic refinement, adding progressively more intricate detail and beauty to the flower-like, ant-like, and rosette-shaped motifs (see, Figures 2–31). It is observed that this parametric manipulation serves as a powerful tool for controlling the visual and structural properties of the fractals. It is seen that

- the parameters  $p, q, \ell, \Psi, \Phi, \omega, \eta$  and  $s$  play a very important role in giving shape, size, and colour to the fractals.
- the convergence criteria derived for the fractals are also playing a very crucial role in determining the resolution and richness of the pixels in the fractals.
- all the fractals developed in this paper are very novel, aesthetic, and pleasing as the complex functions  $\mathcal{U}(z)$  and  $\mathcal{V}(z)$ .

## 5. Conclusion

This study established a novel escape criterion founded on the viscosity approximation iterative method with  $s$ -convexity, specifically developed for the complex rational maps  $\mathcal{U}(z)$  and  $\mathcal{V}(z)$ . Within this theoretical framework, Julia and Mandelbrot sets were computationally generated and visualized using Algorithms 1 and 2, and Algorithms 3 and 4, respectively. MATLAB software was employed to generate these fractals under varying parameter values, revealing intricate and non-classical structures. Employing MATLAB software, we successfully generated a series of compelling non-classical fractal variants as Julia and Mandelbrot sets, which were subsequently discussed and evaluated for various parameter values. Our findings show that parameters such as  $\ell, \Psi, \Phi, \omega, \eta, \wp, \hbar$  and  $s$  and the exponents  $p$  and  $q$  significantly influence the shape, color, and complexity of the fractals—even small variations lead to noticeable changes. These results not only highlight the mathematical depth of the study but also underscore the powerful fusion of computational techniques and creative expression. Furthermore, we believe that the insights garnered from this research will inspire and motivate researchers and enthusiasts deeply engaged in the field of fractal geometry. Future research will focus on extending this work through generalizations involving modified rational exponential and sine functions, and will incorporate quantitative metrics such as computational generation time and the Average Number of Iterations (ANI) into the analysis. The visual richness and diversity of the generated fractals also point to potential applications in the textile industry, especially in pattern design and printing.

## Acknowledgement

The authors gratefully acknowledge Qassim University, represented by the Deanship of Graduate Studies and Scientific Research, on the financial support for this research under the number (QU-J-UG-2-2025-56258) during the academic year 1446 AH/2024 AD.

## REFERENCES

1. I. Ahmad, M. Sajid and R. Ahmad, *Julia sets of transcendental functions via a viscosity approximation-type iterative method with  $s$ -convexity*, Stat., Optim. Inf. Comput., vol. 12, pp. 0–19, 2024.
2. S. Antal, A. Tomar, D.J. Parjapati and M. Sajid, *Fractals as Julia sets of complex sine function via fixed point iterations*, Fractal Fract., vol. 5, pp. 1–17, 2021.
3. A. Husain, M. N. Nanda, M. S. Chowdary, M. Sajid, *Fractals: An Eclectic Survey, Part-I*, Fractal Fract., vol. 6, no. 89, 2022.
4. L. Jolaoso, S. Khan and K. Aremu, *Dynamics of RK iteration and basic family of iterations for polynomiography*, Mathematics, vol. 10, no. 18, 3324, 2022.
5. G. Julia, *Memoire sur l'iteration des fonctions rationnelles*, J. Math. Pures Appl., vol. 8, pp. 47–245, 1918.
6. S. Kumari, K. Gdawiec, A. Nandal, M. Postolache and R. Chugh, *A novel approach to generate Mandelbrot sets, Julia sets and biomorphs via viscosity approximation method*, Chaos Solit. Fractals, vol. 163, pp. 112–140, 2022.
7. S. Kumari, K. Gdawiec, A. Nandal, N. Kumar and R. Chugh, *On the viscosity approximation type iterative method and its non-linear behavior in the generation of Mandelbrot and Julia sets*, Numer. Algorithms, vol. 2023, 2023.
8. Y. C. Kwun, M. Tanveer, W. Nazeer, K. Gdawiec, and S. M. Kang, *Mandelbrot and Julia sets via Jungck-CR iteration with  $s$ -convexity*, IEEE Access, vol. 7, pp. 12167–12176, 2019.
9. P. Maingé, *The viscosity approximation process for quasi-nonexpansive mappings in Hilbert spaces*, Comput. Math. with Appl., vol. 59, no. 1, pp. 74–79, 2010.
10. P. Maingé, *The viscosity approximation process for quasi-nonexpansive mappings in Hilbert spaces*, Comput. Math. with Appl., vol. 59, no. 1, pp. 74–79, 2010.
11. A. Maudafi, *Viscosity approximation methods for fixed-points problems*, J. Math. Anal. Appl., vol. 241, no. 1, pp. 46–55, 2000.
12. P. Muthukumar and P. Balasubramaniam, *Feedback synchronization of the fractional order reverse butterfly-shaped chaotic system and its application to digital cryptography*, Nonlinear Dyn., vol. 74, pp. 1169–1181, 2013.
13. K. Nakamura, *Iterated inversion system: An algorithm for efficiently visualizing Kleinian groups and extending the possibilities of fractal art*, J. Math. Arts, vol. 15, no. 9, pp. 106–136, 2021.
14. A. Nandal, R. Chugh and M. Postolache, *Iteration process for fixed point problems and zero of maximal monotone operators*, Symmetry, vol. 11, no. 5, pp. 655, 2019.
15. P. C. Ouyang, K. W. Chung, A. Nicolas and K. Gdawiec, *Self-similar fractal drawings inspired by M. C. Escher's print square limit*, ACM Trans. Graphic., vol. 40, pp. 1–34, 2021.
16. M. Pinheiro,  *$s$ -convexity, foundations for analysis*, Differ. Geom. Dyn. Syst., vol. 10, pp. 257–262, 2008.

17. W. Phuengrattana and S. Suantai, *On the rate of convergence of Mann, Ishikawa, Noor and SP-iterations for continuous functions on an arbitrary interval*, J. Comput. Appl. Math., vol. 235, no. 9, pp. 3006–3014, 2011.
18. S. Rawat, D.J. Prajapati, A. Tomar and K. Gdawiec, *Generation of Mandelbrot and Julia sets for generalized rational maps using SP-iteration process equipped with  $s$ -convexity*, Math. Comput. Simul., vol. 220, pp. 148–169, 2024.
19. A. A. Shahid, W. Nazeer and K. Gdawiec, *The Picard-Mann iteration with  $s$ -convexity in the generation of Mandelbrot and Julia sets*, Monatsh. Math., vol. 195, pp. 565–584, 2021.
20. M. Tanveer, W. Nazeer and K. Gdawiec, *New escape criteria for complex fractals generation in Jungck-CR orbit*, Indian J. Pure Appl. Math., vol. 51, pp. 1285–1303, 2020.
21. G. I. Usurelu, A. Bejenaru and M. Postolache, *Newton-like methods and polynomiographic visualization of modified Thakur processes*, Int. J. Comput. Math., vol. 98, pp. 1049–1068, 2021.